



Contents lists available at ScienceDirect

Arabian Journal of Chemistry

journal homepage: www.ksu.edu.sa

Original article

Synthesis, Characterization, Antimalarial, Antimicrobial, and antioxidant activities of GNPs with *Annona muricata* leaf extract

Najlāa S. Al-Radadi*

Department of Chemistry, Faculty of Science, Taibah University, P.O. Box 30002, Al-Madinah Al-Munawarah 14177, Saudi Arabia



ARTICLE INFO

Keywords:

Gold Nanoparticles
Annona muricata
 Antimalarial
 Antimicrobial
 Antioxidant

ABSTRACT

The present study is perilous to identify a quick, safe, affordable, and environmentally friendly method to synthesize nanoparticles from plant source. This is due to the extremely detrimental impacts connected to the chemical synthesis of nanoparticles. Therefore, the tropical plant species *Annona muricata* (*A. muricata*) which is a member of the Annonaceae family has numerous therapeutic applications. According to the present studies, the gold nanoparticles (GNPs) were synthesized by the green synthesis method using an aqueous extract of *A. muricata*. The characterizations of synthesized *A. muricata*-GNPs was obtained by different analytical techniques including UV-visible (UV-vis), Fourier Transformed Infrared (FTIR), Transmission Electron Microscopy (TEM), X-ray diffraction (XRD), Energy dispersive X-ray (EDX), and X-Ray Photon Spectroscopy (XPS) analysis. The successful synthesis of GNPs was identified by Surface Plasmon Resonance (SPR) peaks at 532 nm. FT-IR revealed functional groups crucial for nanoparticle formation. TEM confirmed the spherical morphology, while XRD analysis highlighted the crystalline structure. The EDX and XPS analysis determined the elemental and chemical composition of GNPs, respectively. Furthermore, *A. muricata*-GNPs demonstrated promising anti-malarial activity against *P. berghei* and *P. falciparum*, with significant inhibition at maximum concentrations up to 4000 mg/kg. The synthesized GNPs showed significant antibacterial potentials towards both Gram-negative and Gram-positive bacterial strains by using an agar-well diffusion method which demonstrates highest level of inhibition for *Pseudomonas aeruginosa* (ATCC 27853). The ABTS assay was used to evaluate the antioxidant properties of GNPs that revealed maximum activity at IC₅₀ of 96.4 µg/mL. Thus, the aim of the current study is to synthesize *A. muricata*-GNPs and then to explore their antimalarial, antimicrobial, and antioxidant activity that can be used as new prospects in industrial biotechnology.

1. Introduction

Nanotechnology is a fast-growing scientific field with a wide range of potential applications in energy, environmental, industrial, and medical areas (Al-Radadi, 2024a, Ahmed et al., 2019; Ahmed and Al-Radadi, 2020; Ahmed and Al-Radadi, 2020). The synthesis and manipulation of nanoparticles with sizes ranging from 1-100 nm is termed as nanotechnology (Al-Radadi 2022a., Al-Ahmed et al., 2020, Abdullah et al., 2022). The distinctive features of nanoparticles are extremely significant becet al., 2019, ause of their electrical, physiochemical, and magnetic characteristics (Cho et al., 2008, Boroumand Moghaddam et al., 2015, Al-Radadi 2018, Mitchell et al., 2021, Mughal et al., 2021, Al-Radadi and Abu-Dief 2022). Nanoparticles are synthesized from noble metals (Rodrigues et al., 2019, Soleimani Zohr Shiri et al., 2019, Attarilar et al., 2020, Luo et al., 2021, Al-Radadi 2022b) and have potential to serve as

multipurpose agents like diagnostic, remedial agents, and can also be used in drug delivery (Anderson et al., 2019, Basavegowda and Baek 2021, Desai et al., 2021, Lachowicz et al., 2021, Xu et al., 2022). Gold is the most stable metal nanoparticle (Dung et al., 2021, Al-Radadi 2022c, Khan et al., 2022, Maraming et al., 2022) that has different medical applications which can be used in cancer treatment (Elahi et al., 2018, Balfourier et al., 2020, Javed et al., 2020, Singh and Mijakovic 2021, Al-Radadi et al., 2022) Different physical and chemical methods are used to synthesize gold nanoparticles but these methods requires chemical reagents that produces toxic products that may be harmful to living organisms and environment (Dong et al., 2020, Tyagi et al., 2021, Abid et al., 2022, Al-Radadi 2022d). The green synthesis of nanoparticles using biological sources (microorganisms, plants, and agricultural waste) is a sustainable and eco-friendly alternative to traditional chemical methods (Faisal et al., 2021, Amani et al., 2022, Shabani et al.,

* Corresponding author.

E-mail addresses: nsa@taibahu.edu.sa, nsor26@hotmail.com.<https://doi.org/10.1016/j.arabjc.2024.106081>

Received 26 April 2024; Accepted 7 December 2024

Available online 13 December 2024

1878-5352/© 2024 The Author(s). Published by Elsevier B.V. on behalf of King Saud University. This is an open access article under the CC BY-NC-ND license (<http://creativecommons.org/licenses/by-nc-nd/4.0/>).

2023). Recently, green synthesis using plant extract is a less hazardous more sustainable, and environmentally friendly method of synthesizing gold nanoparticles (Al-Radadi 2019, Al-Radadi and Adam 2020, Al-Radadi 2021a, Al Jahdaly et al., 2021, Bharadwaj et al., 2021, Al-Radadi 2022e). Thus, the extensive survey of literature revealed that *Annona muricata*-GNPs is never reported for the synthesis of GNPs. Herein, in this article we are reporting green synthesis of gold nanoparticles by using leaves extract of *Annona muricata* and its therapeutic applications for the first time.

The *Annona muricata* L, a tropical evergreen tree of fruit belongs to the family Annonaceae that is cultivated in the environment of tropical and subtropical and are found in the rainforests of South America and Africa. It is also known as graviola, soursop, and guanabana (Paarakh et al., 2009, Gajalakshmi et al., 2012, Pieme et al., 2014, Mutakin et al., 2022). Traditional healers used various parts of *A. muricata*, particularly the leaves, for ethnomedical purposes to treat plenty of illnesses, such as malaria, cancer, diabetes, abscesses, and liver diseases (Abdul Wahab et al., 2018, Rady et al., 2018, Attarilar et al., 2020, Chan et al., 2020). It can be used as an antidiabetic (Chowdhury et al., 2021, Son et al., 2021), antimicrobial (Costa et al., 2009), antioxidant (Choi and Ohk 2017, Balderrama-Carmona et al., 2020). Although, *A. muricata* leaves contain natural compounds such as phenolic (PL), alkaloids (ALK), acetogenins, and annonaceous acetogenins (AGEs) are the main compound found within the extracts, which contain 212 bioactive compounds (Moghadamtousi et al., 2015, Daud et al., 2016, Coria-Téllez et al., 2018, Nguyen et al., 2020). The long-chain (C-32/C34) fatty acids are a special class of secondary metabolites C-35/C37 in the polyketide pathway that are derived from AGEs (García Durán et al., 2021). Hence, different drug resistance are used to inhibits the possibilities for treating malaria that are among the world worst infectious diseases (Haldar and Mohandas 2009, Parija and Praharaj 2011). Chloroquine (CQ) is a drug used to prevent and treat malaria (Nuwaha 2001) because of its detrimental side effects (Mohammed et al., 2013). The drug resistance exits for different diseases including shortness of breath, Blurred vision, loss of appetite, abdominal convulsions, muscle weakness, bleeding, hearing and mental problems (Carvalho 2020), Therefore, it is necessary to implement an advanced treatment that facilitates the delivery of therapeutics to specific target sites and minimizes side effects of drugs. Furthermore, GNPs have a significant Surface Plasmon Resonance (SPR) and are used extensively in antimalarial therapy (Shmarakov et al., 2017), because of their stability, size, and high surface area-to-volume ratios (Sharma et al., 2016) Furthermore, GNPs have different distinct properties in terms of sensitivity, stability, and targeting effects, introducing them as an antimalarial agent to kill the malaria parasite can increase the effectiveness of malaria medications (Balasubramanian et al., 2010). It is also known that the size, surface functionality, and aggregation state are some of the factors that affect GNPs. It has been determined that GNPs are more detrimental damage the DNA, oxidative stress, inflammatory reactions, and cell death (Al-Radadi 2021b, Mishra et al., 2023). Moreover, gold nanoparticles have a lower environmental risk compared to other engineered nanoparticles, but caution is advised due to potential increased environmental impact from interactions with other contaminants (Hlavkova et al., 2020; Al-Radadi et al., 2024). The bacterial strains such as *Plasmodium falciparum* (*P. falciparum*) and *Plasmodium berghei* (*P. berghei*) exhibit the biological activities of AGEs with no toxicity and increased survival times. (Asase et al., 2012, Somsak et al., 2016, Gavamukulya et al., 2017, Al et al., 2022). The highest inhibition values are observed for *A. muricata*-GNPs towards both Gram-negative and Gram-positive bacteria demonstrating an excellent antibacterial activity (Vijayameena et al., 2013, Makeri et al., 2015, Abdulsalami et al., 2016, Iyanda-Joel et al. 2019). The green synthesized GNPs have shown efficacy against human pathogens and making them the ideal option for drug delivery because of their small size which have ability to enter cells and interact with various molecules without harming any harmful effect (Folorunso et al., 2019, Badeggi et al., 2020, Priya MR and Iyer 2020, Sargazi et al., 2022). Therefore, the present

study proposed an inexpensive, a simple, and environmentally-safe method used to synthesize GNPs using *A. muricata* leaves extract that act as a reducing and stabilizing agent for the very first time. Herein, in this article, we are reporting the synthesis of GNPs using green source method and to then to explore a series of assays that were use to examine the effectiveness of green source synthesize GNPs in term of antimalarial, antimicrobial, and antioxidant activity.

2. Materials and method

2.1. Preparation of *a. Muricata* leaf extract and biosynthesis of *a. Muricata* mediated GNPs

The iHerb website was used for ordering the *A. muricata* leaves and $\text{HAuCl}_4 \cdot 3\text{H}_2\text{O}$ was purchased from Sigma Aldrich. To prepare the *A. muricata* leaves extract, 50 mL of distilled water was heated to a temperature of 70 °C-100 °C. The heater was subsequently switched off, and one *A. muricata* capsule that was equivalent to 1 g was added to distilled water while being constantly stirred. The extract was then allowed to cool for 2 min before being immediately filtered, and the mixture was diluted with (20 mL) distilled water. To synthesize *A. muricata*-GNPs, 6 mL of extract (filtrate) was mixed into 4 mL of $\text{HAuCl}_4 \cdot 3\text{H}_2\text{O}$ (10^{-3}) M solution that was previously prepared. After that, the reaction solution was left to stand in approximately 3 h. The color of the solution turned ruby red, which indicates the formation of *A. muricata*-mediated GNPs. The usual ruby red color of the solution showed that the Au^{+3} ions in the *A. muricata* extract had reduced to Au^0 as a result of the antioxidants present in an aqueous extract.

2.2. Optimization studies for *a. muricata*-GNPs synthesis

Different parameters were studied to evaluate the optimal conditions used for *A. muricata*-GNPs synthesis. These factors included the volume of $\text{HAuCl}_4 \cdot 3\text{H}_2\text{O}$ solution, the volume of *A. muricata* extract, temperature, pH, and time. The resulting solution was used to confirm the synthesis of nanoparticles that were analyzed by TEM analysis and UV-visible absorption spectrometer.

2.2.1. Optimization of extract volume

The optimization of extract volume was carried out by varying volumes of an aqueous plant extract by mixing *A. muricata* extract solution of 1 mL to 6 mL into 4 mL of $\text{HAuCl}_4 \cdot 3\text{H}_2\text{O}$ with (10^{-3}) M solution, respectively. The temperature of the reaction was then kept for approximately 3 h at RT 25 °C.

2.2.2. Optimization of $\text{HAuCl}_4 \cdot 3\text{H}_2\text{O}$ volume

The volume impact of $\text{HAuCl}_4 \cdot 3\text{H}_2\text{O}$ solution was investigated by sequentially mixing 1 mL to 6 mL volumes of $\text{HAuCl}_4 \cdot 3\text{H}_2\text{O}$ solution to 4 mL of *A. muricata* extract for approximately 3 h at RT 25 °C.

2.2.3. Optimization of reaction time

The UV-vis absorbance for *A. muricata*-GNPs was obtained from the reaction medium with an optimal volume of $\text{HAuCl}_4 \cdot 3\text{H}_2\text{O}$ solution and *A. muricata* extract. The final solution was monitored with different contact times at room temperature (25 °C), ranging from 30 to 180 min. This type of study facilitates the effect of the reaction time.

2.2.4. Optimization of pH

The pH parameters used for the reaction medium were evaluated with pH levels, notably 2, 4, 6, and 8, following a 3-hour reaction time and at room temperature (RT 25 °C) with optimized volumes of *A. muricata* extract and $\text{HAuCl}_4 \cdot 3\text{H}_2\text{O}$ solution were used.

2.2.5. Optimization of temperature

To obtain the *A. muricata*-GNPs synthesis, the reaction was optimized by keeping the reaction at different temperatures between 15–35 °C for

Table 1

Impact of *A. muricata* Extract, *A. muricata*-GNPs, and Chloroquine on Body Weight Changes Under Different Experimental Infected Mice Groups.

Treatment groups	Body weight (g) 0 day	Body weight (g) 7 days	Body weight (g) 14 days	Body weight (g) 21 days
Negative Control	30 gm	31 gm	32 gm	33 gm
Positive Control	25 g	28 g	30 g	33 g
Chloroquine (12 mg/kg)	35 g	33 g	29 g	26 g
<i>A. muricata</i> (200 mg/kg)	29 g	30 g	32 g	35 g
<i>A. muricata</i> (800 mg/kg)	28 g	30 g	33 g	36 g
<i>A. muricata</i> -GNPs (10 µg/g)	32 g	34 g	36 g	38 g
<i>A. muricata</i> -GNPs (40 µg/g)	31 g	32 g	34 g	36 g

approximately 3 h.

2.3. Characterization of biosynthesized GNPs

The research investigation analyzed the morphological, structural, and vibrational properties of biosynthesized graphene nanoparticles (GNPs) via different analytical techniques, such as X-ray Photoelectron Spectroscopy, Zeta Potential, X-ray Diffraction pattern, Energy Dispersive X-ray Spectroscopy, UV-visible, Fourier Transform Infrared Spectroscopy, Transmission Electron Microscopy, and High-Resolution Transmission Electron Microscopy. analysis. The phytochemicals along with their functional groups present in GNPs were identified by using FTIR spectroscopy ($400\text{--}4000\text{ cm}^{-1}$). XRD (Model D8 Advance, Germany) was used to determine the crystal-like characteristics, phase identification, and purity of GNPs. The morphological properties of the GNPs were computed by using Transmission Electron Microscopy. X-ray Photoelectron Spectroscopy was used to provides strong evidence against the surface morphology of *A. muricata*-GNPs.

2.4. Antimicrobial activity

2.4.1. Agar-Well diffusion method

The method of Agar well dispersion was used to carry out the antimicrobial action of *A. muricata*-GNPs. The selected microbial strains were collected from the Mansour Scientific Foundation for Research and Development (MSF), Jeddah, Saudi Arabia. In this analysis, the Petri plate was divided into a 5 mm range well and brooded for 72 h at room temperature and 24 h at 37 °C to stimulate the growth of microbial strains. The shift in the obstruction zone was calculated by measuring the width in millimeters. In this experiment, the bacterial and fungal strains that were inoculated with a spreader were added to the well with different concentrations of test samples, respectively. The immersion of the test samples in DMSO did not show any inhibition activity against microbial cultures, indicating the adverse effect on growth of microbial species. After that, the selected strains were extended on culture media, incubated at 37 °C for 24 h, and the inhibition zone was measured at triplicate of the experiment.

2.4.2. Antibacterial activity

The strength of antibacterial activity of *A. muricata*-extract and *A. muricata* -GNPs was evaluated by using Gram-negative strains of bacteria such as, *Escherichia coli*, *klebsiella pneumonia*, and *Pseudomonas aeruginosa*, and Gram-positive strains of bacteria are *Bacillus subtilize*, *Staphylococcus aureus*, and *Staphylococcus mutants*.

2.4.3. Antifungal activity

The antifungal activity of the *A. muricata*-extract and *A. muricata*-GNPs was assessed against three fungal strains: *A. flavus*, *Aspergillus nigra*, and *Candida albicans*.

2.5. Antimalarial assay

2.5.1. Preparation of aqueous leaf extract

In this analysis, 7 g of *A. muricata* powder was mixed into 100 mL of distilled water to formulate the *A. muricata* aqueous leaves extract and the mixture was heated for 5 min. After filtering the mixture, the aqueous *A. muricata* extract of leaves was kept at $-6\text{ }^{\circ}\text{C}$ until required.

2.5.2. Preparation of GNPs dose concentrations

Phosphate buffer saline (PBS) was used to dissolve the GNPs which were prepared daily at low doses of 10 µg /g/day (low dose), and high doses of 40 µg/g/day.

2.5.3. Experimental animals

Female ICR Swiss albino mice, weighing 25–30 g (aged 4 weeks) were used in this study (Table 1). All animal procedures were conducted in accordance with the ethical guidelines of the institutional animal care and use committee and were approved the Mansour Scientific Foundation for Research and Development (MSF), Jeddah, Saudi Arabia. The study adhered to all relevant regulations and guidelines for the humane care and use of animals in research. The mice were maintained on standard conditions ($20 \pm 2\text{ }^{\circ}\text{C}$, 50–70 % relative humidity, and 12-h light/dark cycle). The animals were provided with a commercial diet and water *ad libitum*. The animals were left for one week for acclimation. Animal experiments were designed and conducted according to the guidelines of the institutional animal ethical committee. After that, mice were divided into 13 groups: one for the negative control group (normal diet), one for the Chloroquine (CQ) group, two *A. muricata* dose extract groups (one low dose of 200 mg/kg and one high dose of 800 mg/kg), two *A. muricata*-GNPs dose groups (one low dose 10 µg/g and one high dose 40 µg/g), and one for the positive control group (G7).

2.5.4. Acute toxicity assay

A modified Lorke's method was used to test the acute toxicity of leaf extract of *A. muricata* (Lorke 1983). In this analysis, 24 female ICR mice were randomized into 8 groups of 3 mice each and were then given orally with 100, 500, 1000, 2000, 4000, 5000, 6000,7000 mg/kg. The mice were examined for toxicity symptoms including coma, entire body stretching, salivation, paw licking, weakness, sleep, respiratory distress, and death in the first 4 h and afterward 1–7 days. The oral median lethal dose was calculated using the formula as follows:

$$\text{LD50} = \sqrt{(\text{Minimumtoxicdose} \times \text{Maximumtoleratedose})} \quad (1)$$

2.5.5. Parasites

Blood-stage samples of *Plasmodium berghei* (ANKA) and *Plasmodium falciparum* (PbANKA), were used for mice infection. The parasites were conserved as stabilities of 10×10^6 parasitized red blood cells (pRBCs) stored in liquid nitrogen in solution for cryopreservation of the parasite.

2.5.6. Infection of mice

Except for the healthy control group, all mice were infected intraperitoneally (ip) with either *P. Berghei* (ANKA, 10×10^6) or *P falciparum* (PbANKA, 10×10^6) parasitized erythrocytes. Whereas, the parasitemia was examined under a microscope using a thin blood smear stained with Giemsa, daily (Janse et al., 2006). When the parasitemia reached approximately 5 % of the initial inoculation, treatment groups were assigned. The (% parasitemia) percentage of parasitemia was calculated using the formula as follows:

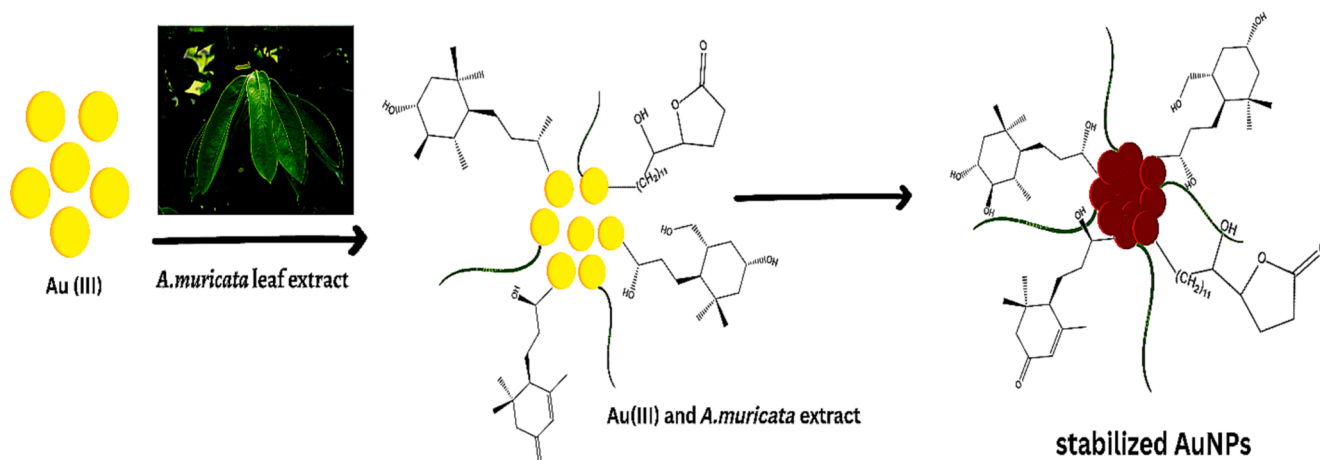


Fig. 1. Schematic illustrations used for the synthesis of *A. muricata*-GNPs using the extract of *A. muricata* and was combined with gold chloride and nanoparticles were synthesized.

$$\% \text{ parasitemia} = \frac{\text{Number of parasitized erythrocytes}}{\text{Number of erythrocytes}} \times 100 \quad (2)$$

2.5.7. Experimental Design

Mice were randomly divided into two classes:

Class I, groups of mice infected with 10×10^6 *P. berghei* (ANKA) consists of seven groups, each of eight mice as follows:

Group (1): Healthy control uninfected group.

Group (2): ANKA- infected mice.

Group (3): ANKA-infected mice treated with an intraperitoneal injection of chloroquine (CQ) (12 mg/kg, ip injection).

Group (4): ANKA-infected mice treated orally with *A. muricata* (200 mg/kg).

Group (5): ANKA-infected mice treated orally with *A. muricata* (800 mg/kg).

Group (6): ANKA-infected mice treated orally with *A. muricata*-GNPs (10 $\mu\text{g/g}$).

Group 7: ANKA-infected mice treated orally with *A. muricata*-GNPs (40 $\mu\text{g/g}$).

Class 2, groups of mice infected with 10×10^6 *P. falciparum* (PbANKA) consists of 6 groups, each of eight mice as follows:

Group 8: PbANKA- infected mice.

Group 9: PbANKA- infected mice treated with intraperitoneal injection of chloroquine (CQ) (12 mg/kg, ip injection).

Group 10: PbANKA- infected mice treated orally with *A. muricata* (200 mg/kg).

Group 11: PbANKA-infected mice treated orally with *A. muricata* (800 mg/kg).

Group 12: PbANKA- infected mice treated orally with *A. muricata*-GNPs (10 $\mu\text{g/g}$).

Group 13: PbANKA – infected mice treated orally with *A. muricata*-GNPs (40 $\mu\text{g/g}$).

All treatments were given daily for 4 consecutive days (Peters et al., 1975). On day 5 of experiment, parasitemia and percentage of inhibition were calculated according to the following formula:

$$\% \text{ inhibition} = \frac{\text{parasitemia of untreated group} - \text{parasitemia of extract treated group}}{\text{parasitemia of untreated group}} \times 100 \quad (3)$$

2.5.8. Determination of packed cell volume

To determine the packed cell volume (PCV) of each mouse, the tail

blood was collected into heparinized hematocrit tubes, sealed with Critoseal, and centrifuged for 5 min at 10,000 rpm (Somsak et al., 2016). Then, using a hematocrit reader, PCV was determined using the following formula:

$$\text{PCV} = \frac{\text{Volume of packed erythrocytes}}{\text{Total volume of blood}} \times 100 \quad (4)$$

2.6. Antioxidant assay

The antioxidant and free radical properties of *A. muricata*-GNPs and *A. muricata* extract were investigated using the ABTS assay (Donga et al., 2020). In a 96-well microtiter plate, the free radicals in the ABTS were neutralized by dissolving methanol into ABTS. After that, various concentrations of plant extract and GNPs were added to a 96-well plate. The plate was then allowed to incubate for 45 min at room temperature in the dark. Ascorbic acid was used as a positive and reference control group. The antioxidant activity of the reaction was determined after it was exposed to an absorbance of 517 nm.

$$\text{ABTS free radical scavenging (\%)} = \frac{\text{control} - \text{test}}{\text{control}} \times 100 \quad (5)$$

2.7. Statistics

The results were analyzed and compared with a 95 % confidence level using the one-way ANOVA. Significant values were defined as $p < 0.05$. The results were expressed as mean \pm standard error of mean (SEM) and comprised data from Presim 9.

3. Results and Discussion

3.1. *A. muricata*-GNPs synthesis under different conditions and its characterization using UV-visible and TEM analysis

The green fabrications of GNPs were achieved under a wide range of

circumstances, including different *A. muricata* extract volumes, $\text{HAuCl}_4 \cdot 3\text{H}_2\text{O}$ solution concentrations, time intervals, and pH levels.

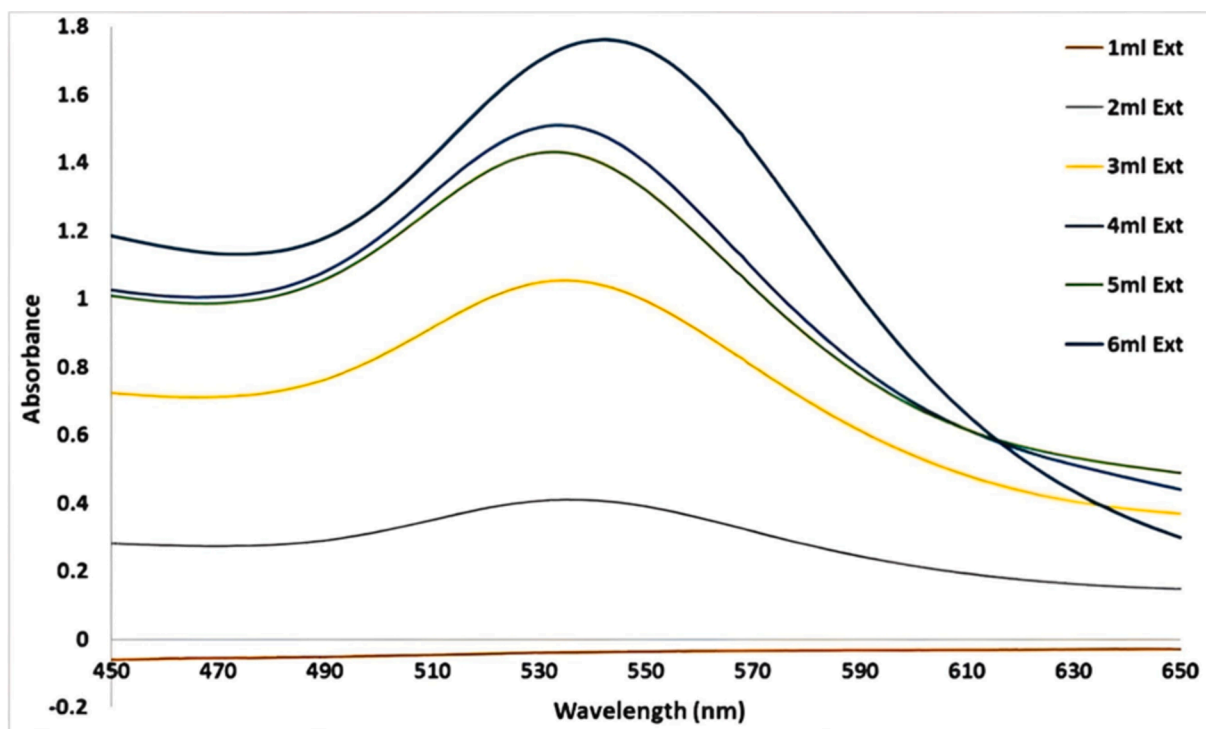


Fig. 2. UV-vis Absorption spectra of *A. muricata*-GNPs under the volumes of *A. muricata* extract 1 to 6 with 4 ml of $\text{HAuCl}_4 \cdot 3\text{H}_2\text{O}$ (10^{-3} M) at RT 25C° after 3 h.

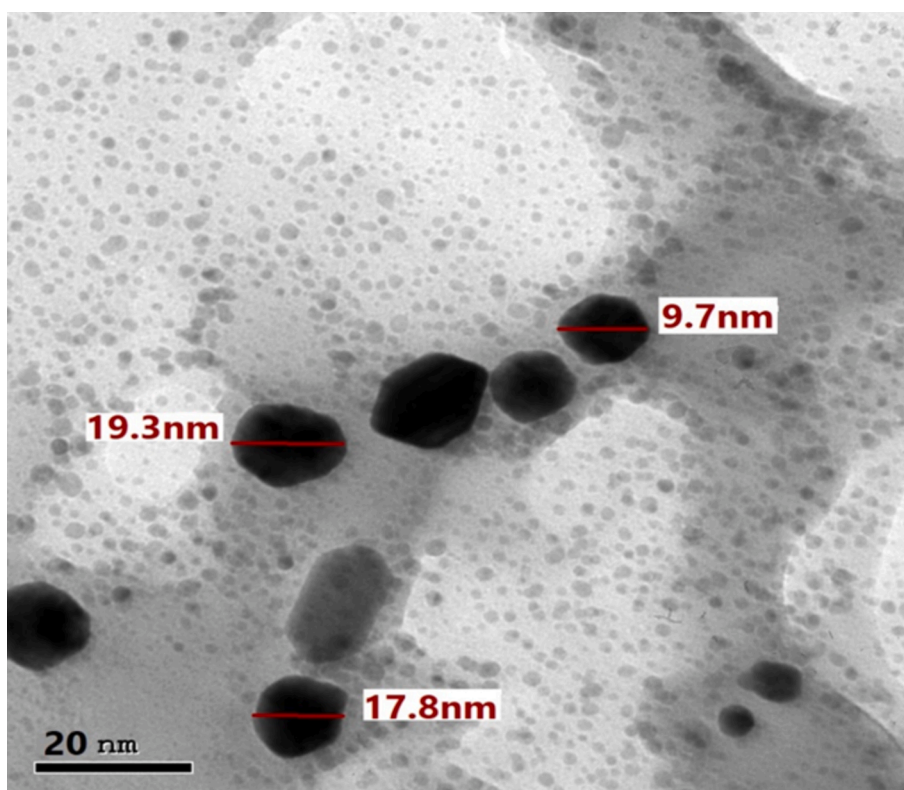


Fig. 3. TEM image of *A. muricata*-GNPs under different volumes extract of *A. muricata*.

Nonetheless, the color shift of the reaction solution to ruby-red indicates the formation of GNPs with the *A. muricata* extract. The first indication for the successful formation of GNPs was the appearance of a ruby-red due to excitation of surface plasmon resonance vibrations in gold nanoparticles. The surface plasmon resonance is a collective excitation

of the electrons in the conduction band around the nanoparticle surface. Electrons conform to a specific vibration mode by particle size and shape. Therefore, metallic nanoparticles display characteristic optical absorption spectra in the UV-vis region. The obtained results showed that *A. muricata*-GNPs displayed a distinctive peak associated with the

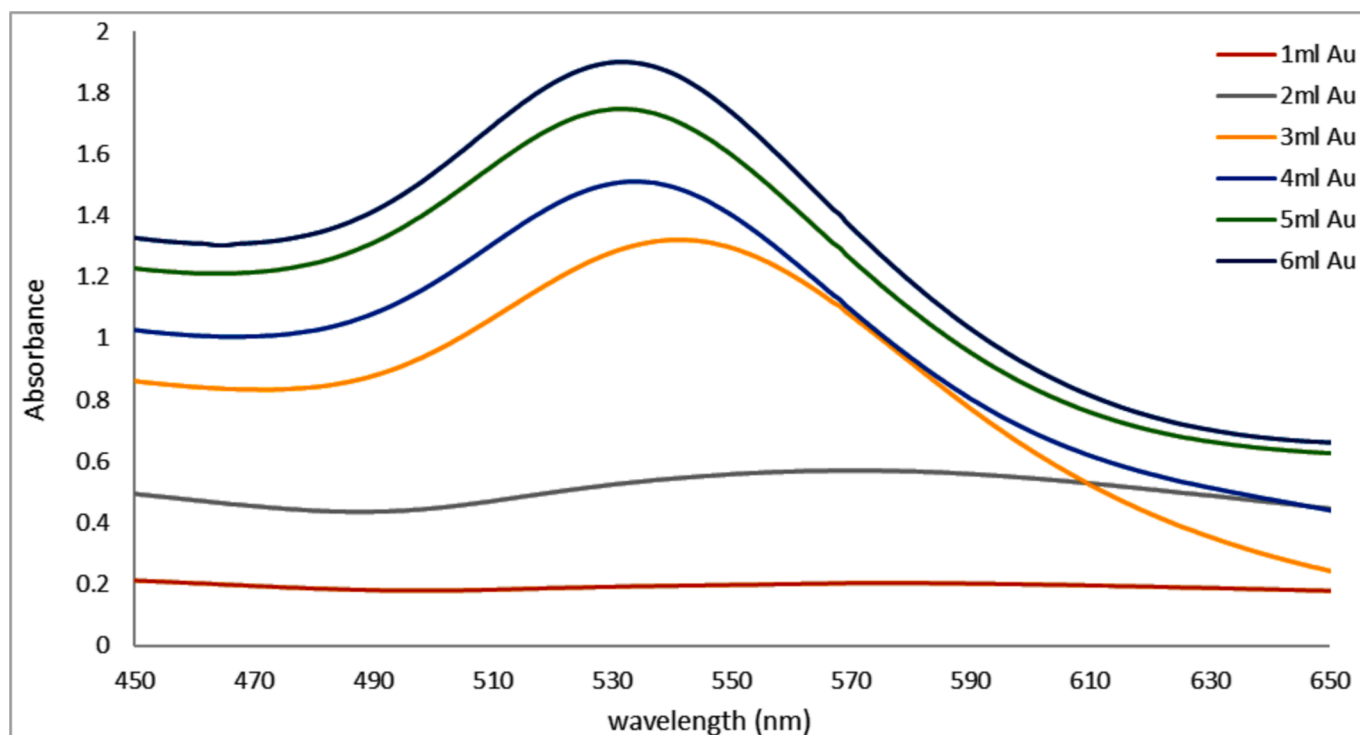


Fig. 4. UV-vis Absorption spectra of *A. muricata*-GNPs under the volumes of HAuCl₄ · 3H₂O (10⁻³ M) 1 to 6 mL with 4 mL of *A. muricata* extract at RT 25°C and after 3 h.

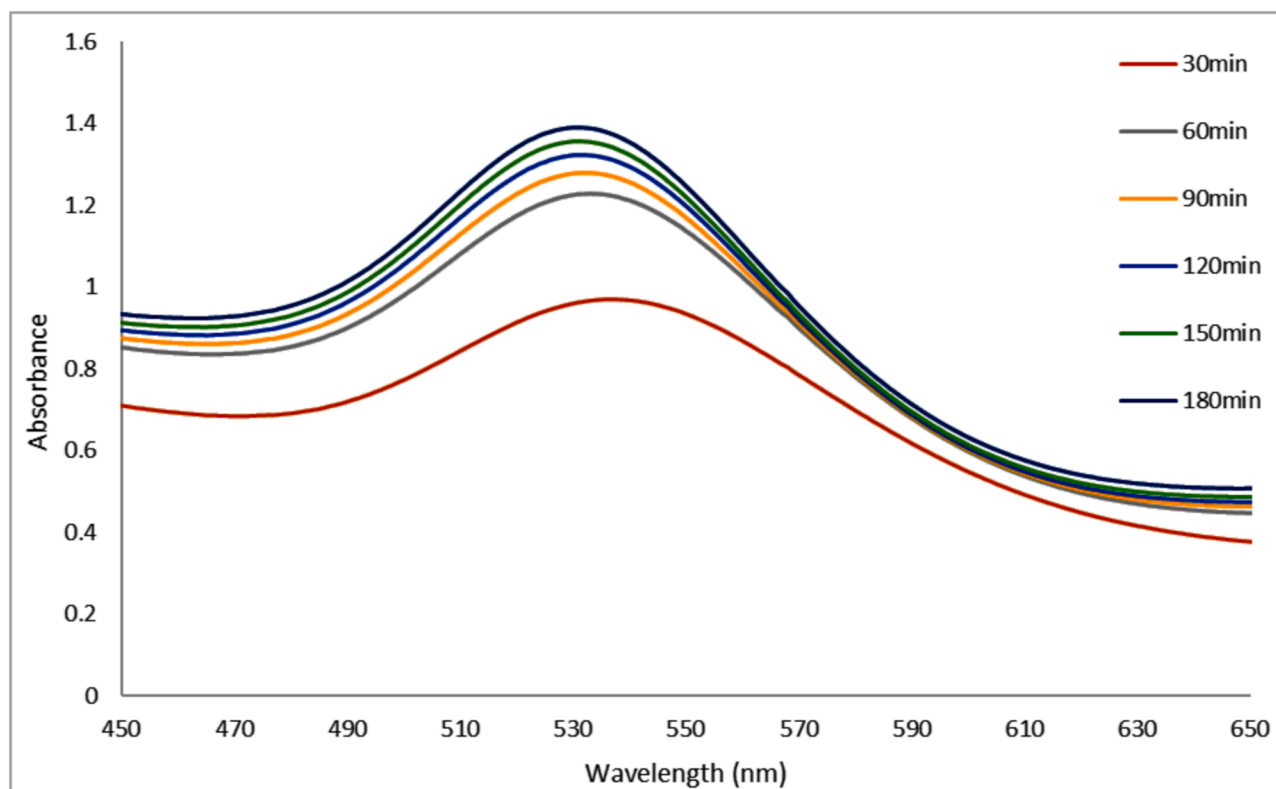


Fig. 5. UV-vis Absorption Spectra of *A. muricata*-GNPs for 4 mL of *A. muricata* extract and 4 mL of HAuCl₄ · 3H₂O (10⁻³ M) at RT 25°C for 180 mins.

absorption of Surface Plasmon Resonance (SPR) at 532 nm. This also shows how the GNPs formed. Furthermore, TEM images of synthesized *A. muricata*-GNPs reinforce the obtained results. The results of current

study were compared to the previous study (Martínez et al., 2012, Al-Radadi 2022b). Furthermore, the exact reaction mechanism is not fully explained due to the complex nature of biomolecules involved in

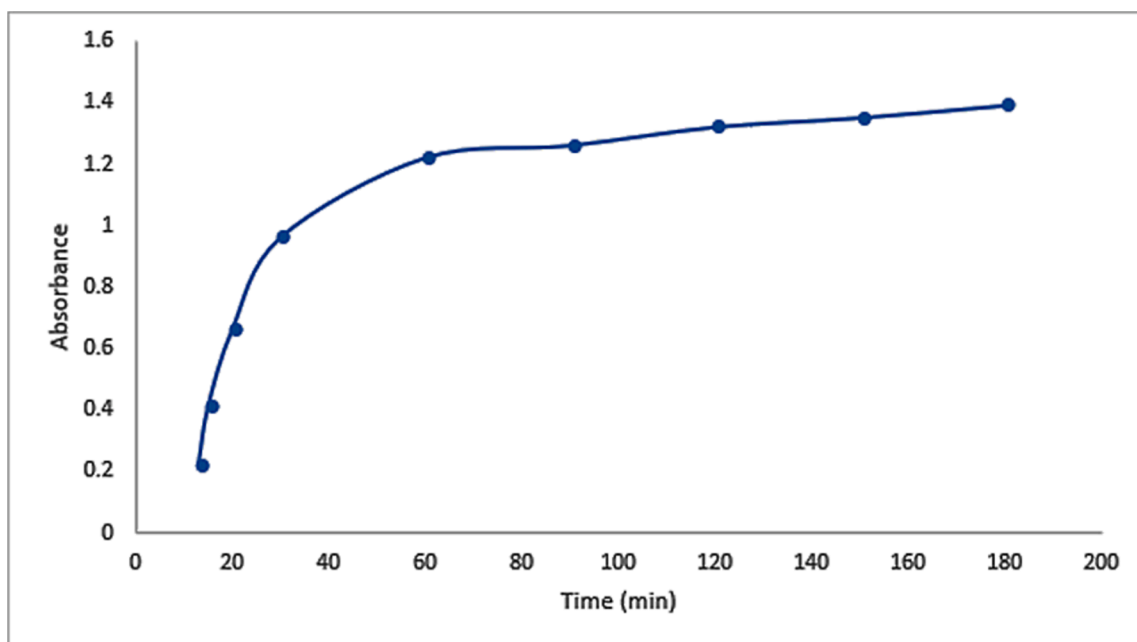


Fig. 6. Variation in intensity in the UV-vis Absorption Spectra of GNPs with time at RT 25 °C using 4 ml of $\text{HAuCl}_4 \cdot 3\text{H}_2\text{O}$ (10^{-3} M) solution and 4 ml of *A. muricata* extract.

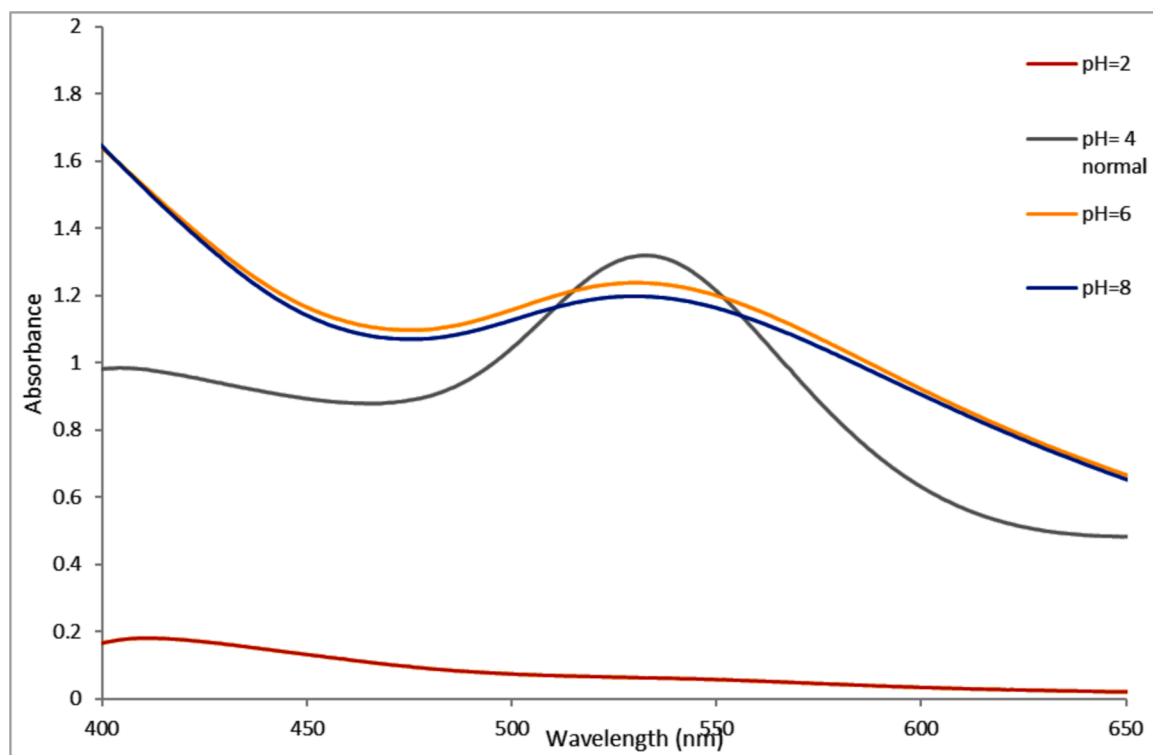


Fig. 7. UV-vis Absorption Spectra of *A. muricata*-GNPs under pH level (2–8) with 4 ml of *A. muricata* extract and 4 ml of $(\text{HAuCl}_4 \cdot 3\text{H}_2\text{O})$ (10^{-3} M) at RT 25 °C, after 3 h.

the reaction. The major involvement of polyphenolic compounds in the green synthesis of GNPs. Moreover, *A. muricata* have been reported to contain 212 bioactive compounds more concentration of polyphenols and flavonoids (Al-Radadi., 2023, Moghadamtousi et al., 2015, Daud et al., 2016, Coria-Télez et al., 2018, Nguyen et al., 2020). Thus, the experimental results suggest a hypothetical reaction mechanism for phenolic compounds which reduce Au^{+3} and stabilizing GNPs using

aqueous *A. muricata* extract. The plant extract of *A. muricata* exhibits strong chelating potency due to its high antioxidant activity and excellent chelating ability, attributed to its higher amount of reducing and stabilizing agents. Various phenolic compounds including alkaloids, acetogenins, and annonaceous acetogenins are responsible for conversion of metallic ions into metal nanoparticles. The reduction of gold ions by bio-compounds involves the oxidation of phenolic compounds. The

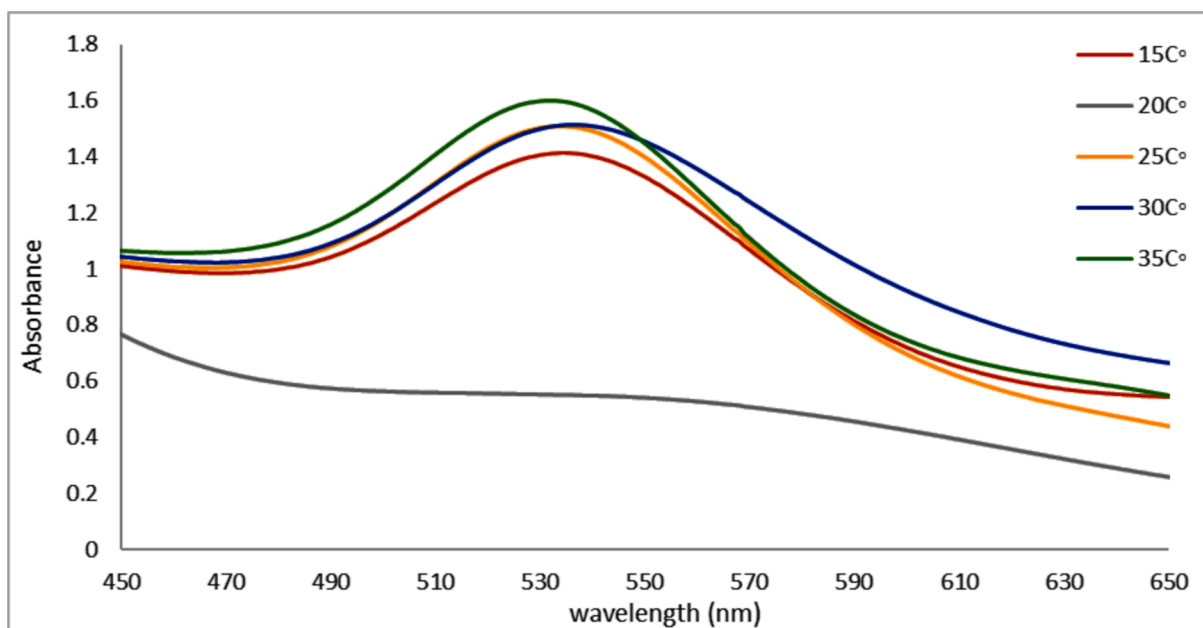


Fig. 8. UV-vis Absorption spectra of *A. muricata*-GNPs with 4 ml of ($\text{HAuCl}_4 \cdot 3\text{H}_2\text{O}$) (10^{-3} M) solution and 4 ml of *A. muricata* extract under different temperatures for 3 h.

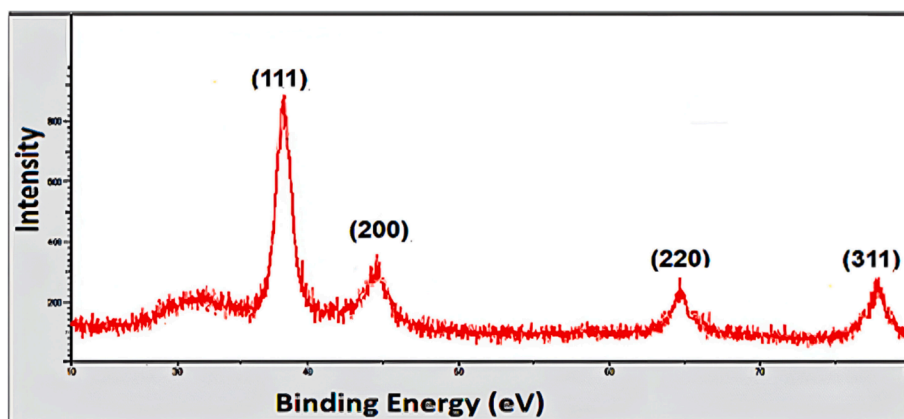


Fig. 9. X-ray diffraction pattern of *A. muricata*-GNPs.

biomolecules move to free orbital gold ions with subsequent formation of gold atoms. Thus, the phenolic compounds first bind to Au^{+3} to form the chelating rings and form stable synthesis of GNPs, as illustrated in (Fig. 1). These interaction leads to enhanced the biological applications of synthesized GNPs.

3.1.1. Effect of extract volume

A. muricata-GNPs reactions were carried out in a series of volumes ranging from 1 mL to 6 mL of leaves extract of *A. muricata* with 4 mL of (1×10^{-3}) of $\text{HAuCl}_4 \cdot 3\text{H}_2\text{O}$ solution constant volume. The color shift to ruby-red was used as a visual cue that the reaction had been happening at room temperature for approximately three hours. According to UV-visible spectra, the SPR peak intensity increased and sharpened as the *A. muricata* extract volume increased from 1 mL to 4 mL, and at 5 mL, the peak decreased, but at 6 mL the peak is hypsochromic shift obtained after 3 h of reactions (Fig. 2). As a result, the optimization parameter revealed that volume of leaves extract of *A. muricata* had significant impact on the synthesis of GNPs. In light of this investigation, an ideal extract volume of *A. muricata* was 4 mL which was appropriate for the synthesis of nanoparticles at 532 nm, which coincides with those of the UV-visible absorption. The results were identified by examining the

TEM results from the optimal *A. muricata*-GNPs (Fig. 3). The findings demonstrated that the GNPs were spherical, with sizes ranging from 24.5 nm to 33.1 nm, and are distributed uniformly without agglomeration. Similar study investigates the volume effect of GNPs in UV-Vis spectroscopy which were consistent to the obtained results (Al-Radadi et al., 2024).

3.1.2. Effect of $\text{HAuCl}_4 \cdot 3\text{H}_2\text{O}$ volume

The volume effect of $\text{HAuCl}_4 \cdot 3\text{H}_2\text{O}$ (10^{-3}) solution on optimum synthesis of GNPs was examined by synthesizing *A. muricata*-GNPs under the volume of $\text{HAuCl}_4 \cdot 3\text{H}_2\text{O}$ (10^{-3}) starting from 1 mL to 6 mL with 4 mL constant volume of *A. muricata* extract for 3 h at RT. The UV-visible and TEM analyses were used to evaluate the optimum synthesis of *A. muricata*-GNPs. When the volume of the $\text{HAuCl}_4 \cdot 3\text{H}_2\text{O}$ was increased to 4 mL, the peaks were hypsochromic shifted. However, the UV-vis spectra for the 2 mL solution exhibit weak peak intensity at about 569 nm. This is due to the concentration of the gold (III) chloride trihydrate complex being diluted when the volume of the $\text{HAuCl}_4 \cdot 3\text{H}_2\text{O}$ solution is increased. The interactions between the surrounding water molecules and the gold (III) ions become weaker. Because the electronic transitions require less energy for causing the absorption peaks and

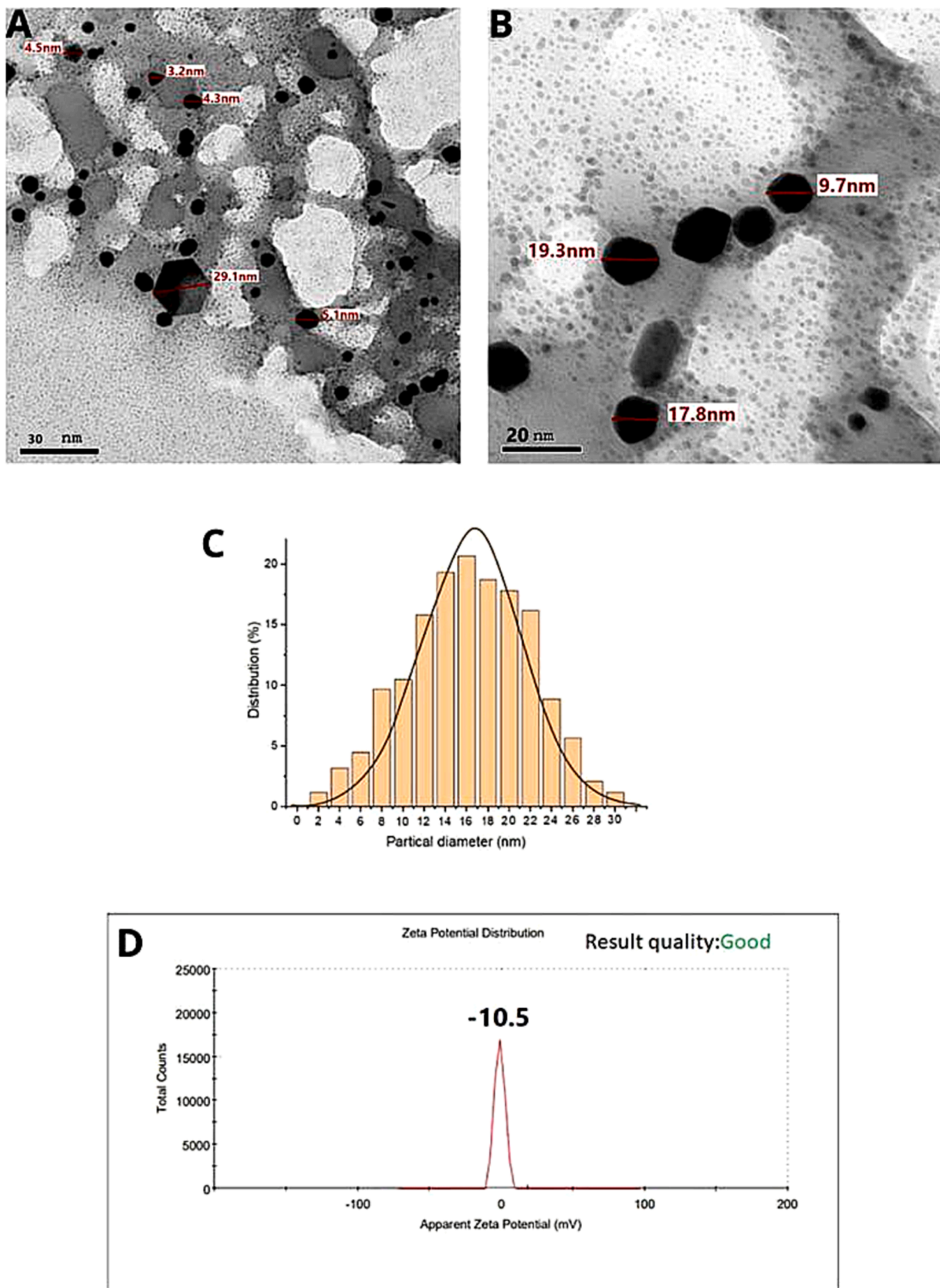


Fig. 10. HRTEM images (A) and (B), and (C) corresponding size distribution graph, (D) Zeta potential of *A. muricata*-GNPs.

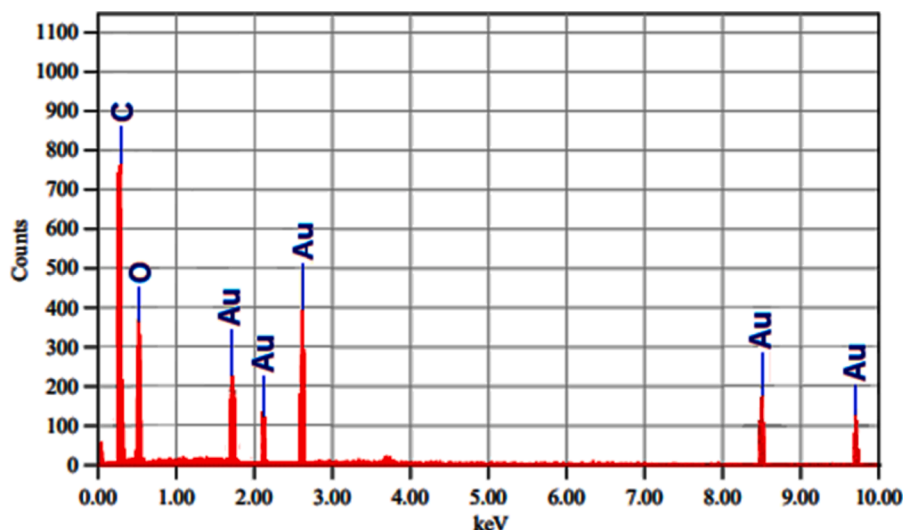


Fig. 11. EDX analysis for *A. muricata*-GNPs.

result a hypsochromic shift in the absorption spectrum. Therefore, the peak shifted to 532 nm by the strong absorption observed in peak intensity (Fig. 4). The TEM analysis revealed comparable results, illustrating a similar shape and size of GNPs without aggregation, as observed in (Fig. 3) (Al-Radadi., 2021b).

3.1.3. Effect of reaction time

The contact time effect was examined by a series of reactions that were carried out at room temperature for up to 180 min (3 h) using 4 ml of $\text{HAuCl}_4 \cdot 3\text{H}_2\text{O}$ (10^{-3}) solution and 4 ml of *A. muricata* extract. UV–vis spectrums were used to track the resulting *A. muricata*-GNPs reactions at one-hour intervals. The clear SPR peaks centered at 180 min at 532 nm were visible in the UV–vis spectra. The intensity of absorption peaks increased with increasing reaction time and becomes stronger and sharper at 180 min (Fig. 5). Additionally, the absorbance plot versus reaction time shows that the SPR peak significantly increases up to 180 min (Fig. 6). This finding suggests that *A. muricata*-GNP interference can cause a fast reaction up to 180 min. The increases in absorbance over time indicate a decrease in metal ions and a concentration of nanoparticles. This was due to the smaller nuclei that reduce particle size, as indicated by an increase in SPR peak intensity. The SPR and colloidal solution remain stable for 180 min. Thus, the synthesized *A. muricata*-GNPs were validated further via TEM analysis and revealed that results were similar to those exhibited in (Fig. 3).

3.1.4. Effect of pH

The pH effect on optimum synthesis of *A. muricata*-GNPs were examined by investigating the reaction medium at different levels, ranging from 2 to 8 pH. The UV spectra were used to record the reactions, and the SPR peak at about 532 nm indicates the formation of *A. muricata*-GNPs. The peak intensity increases from 2 to 4 pH, but the peaks broaden to 6 and 8 pH (Fig. 7). The pH of a solution significantly impacts the size and morphology of GNPs which indicate the high monodisperse and spherical morphology of GNPs with a pH 4, during their synthesis. This demonstrated that the ideal pH for synthesizing *A. muricata*-GNPs is the standard pH 4, which was further supported by TEM analysis in line with the findings of the earlier study (Fig. 3) (Al-Radadi., 2022b).

3.1.5. Effect of temperature

This investigation assessed the impact of temperature on the synthesis of *A. muricata*-GNPs by varying the temperatures of the reaction ranges between 15 and 35 °C for approximately three hours while maintaining the optimized conditions mentioned above to obtain

A. muricata-GNPs. The impact of temperature plays an important role on synthesis of GNPs. *A. muricata*-GNPs synthesis led to a more uniform size distribution and a higher rate of nanoparticle formation as the temperatures of the reaction mixture was increases. This is because higher temperatures accelerate the reduction of precursor gold and the nucleation and growth of the nanoparticles. Thus, the UV spectra of the reaction mixture showed a distinct SPR peak at 532 nm as the temperature increases; the optimum peak was at RT 25 °C (Fig. 8). Thus, the reaction rate increases with optimum (25 °C) that facilitated and enhanced the kinetic energy of the reaction. When the temperatures below the optimum level result in lower yield or slower progress, while temperatures above the optimum level (35 °C) destabilize reactants or products (Al-Radadi., 2022e).

3.2. X-ray diffraction analysis

Powder XRD patterns were used to examine the purity and crystallinity of *A. muricata*-GNPs. The obtained results observed four peaks that were identified in the powder XRD patterns equivalent to the (111), (200), (220), and (311) planes, at diffraction angles 38.1°, 44.51°, 64.61°, and 77.82°, respectively. These peaks correspond to the previously published characteristic powder pattern for GNPs obtained through a green synthesis method. A glassy order state in the *A. muricata* extract may be the cause of the peak observed at approximately 22° diffraction angle. However, *A. muricata*-GNPs achieve an almost crystalline nature as indicated by the peak intensities (Fig. 9). The face-center cubic crystalline structure of GNPs was confirmed from the intense peaks in the XRD pattern. These values agreed well with the reported standards JCPDS file no. 04-0784. Similar results were reported earlier in GNPs (Al-Radadi and Al-Youbi 2018a, Taib et al., 2019). The Debye-Scheerer formula is used to ascertain the average size of crystallites:

$$D = \frac{k\lambda}{\beta \cos\theta} \quad (6)$$

Where the crystalline grain average thickness was represented by D, the Scherrer constant (0.89) corresponds to K, the Full-Width Half Maximum (FWHM) is represented by β , the angle of diffraction is denoted by θ , and λ symbol corresponds the X-ray wavelength.

3.3. TEM and HR-TEM and Zeta-potential analysis

TEM analysis was employed to investigate the morphology and size

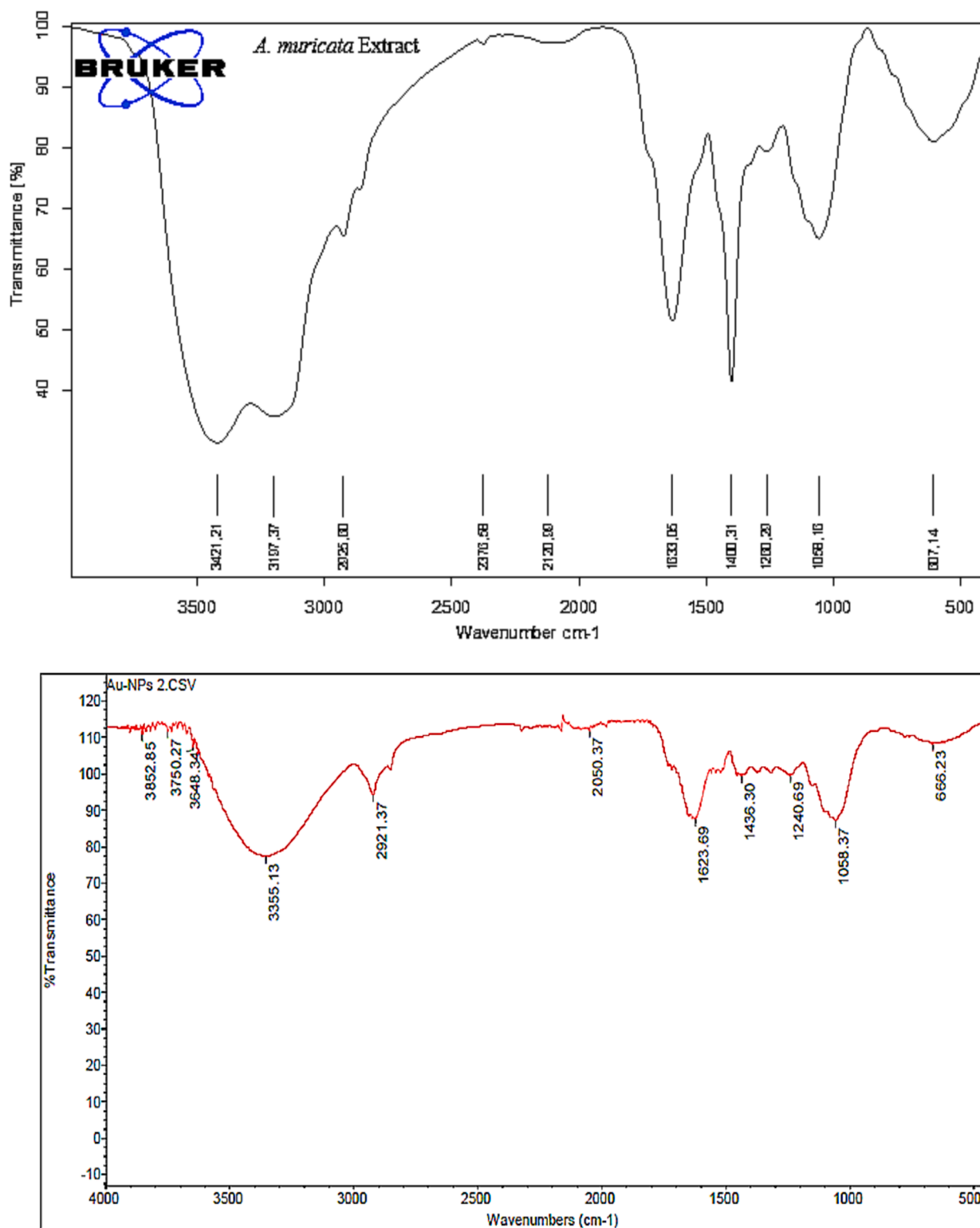


Fig. 12. FTIR spectrum of *A. muricata* Extract and *A. muricata*-GNPs.

dependence of *A. muricata*-GNPs. *A. muricata*-GNP sizes at different ranges were observed in TEM images. *A. muricata*-GNP's TEM images in (Fig. 10A and B) identified the spherical shape morphology with nano size and did not exhibit any aggregation in the synthesized nanoparticles. An additional method for morphological analysis was demonstrated in the TEM micrograph (Fig. 10A and B) which offers an obvious determination for the size of *A. muricata*-GNPs ranges as 47.3 nm to 151.7 nm at 200 nm resolution, and 29.7 nm to 40.1 nm at 50 nm

resolution. In addition, the average particle size distribution histogram was investigated by the intensity peak observed (Fig. 10C). The triplicate analysis revealed an average zeta potential of -10 mV clearly showed that the GNPs were stable at 25 °C (Fig. 10D). Similar results were obtained in the previous reported literature that demonstrate regular morphology and size distribution of GNPs synthesized using green source method (White et al., 2007, Paul et al., 2014, Kajani et al., 2016, Swain et al., 2016).

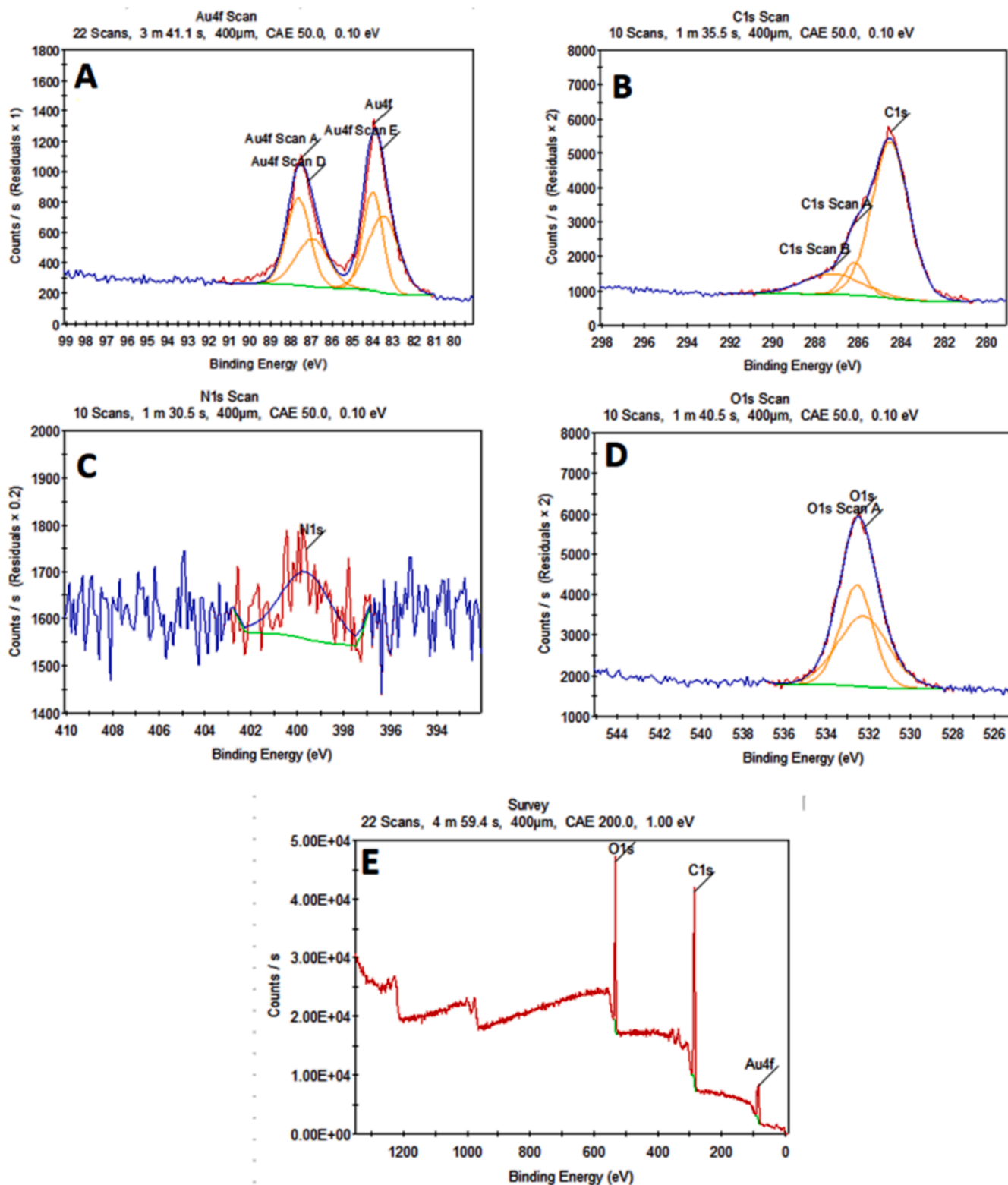


Fig. 13. XPS analysis displaying a survey image (A) Au, (B) Carbon, (C) Nitrogen and (D) Oxygen, (E)survey.

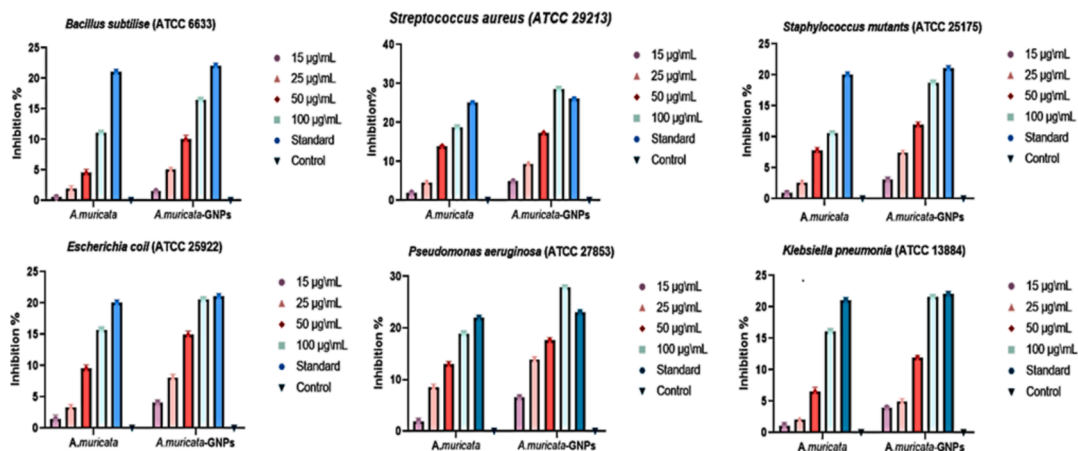
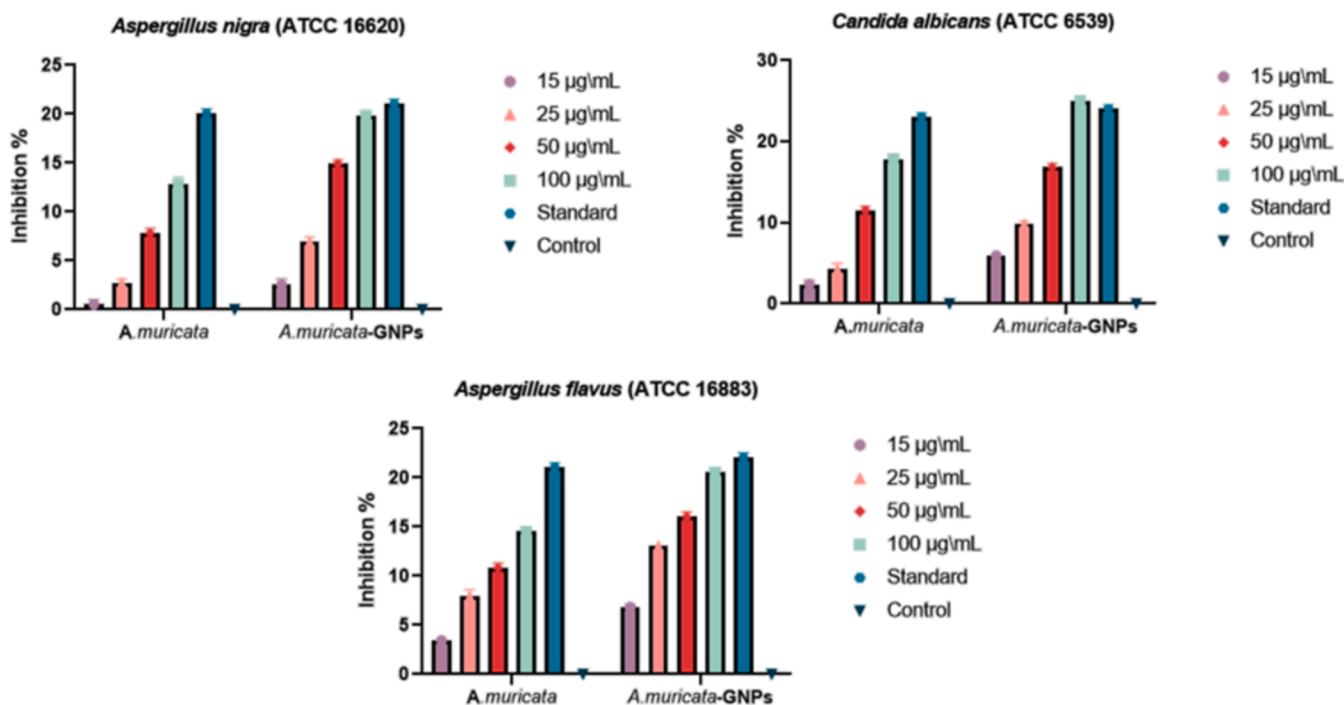
3.4. EDX analysis

The EDX technique was used to carry out elemental characterization of gold. The *A. muricata*-GNPs elemental analysis profile revealed a gold study signal at 2.6 KeV adjacent to peaks for carbon and oxygen (Fig. 11). These light elements (carbon and oxygen) may exist as impurities in samples of gold nanoparticles. However, the detection of

elemental impurities in the GNPs may be hindered by the carbon coating during sample preparation (Al-Radadi and Al-Youbi (2018)b).

3.5. FTIR analysis

FTIR analysis was performed to identify the active groups in the plant extract that act as stabilizing and reducing agent. Fig. 12 displays

Fig. 14. Anti-bacterial potential of *A. muricata* and *A. muricata*-GNPs.Fig. 15. Antifungal potential of *A. muricata* and *A. muricata*-GNPs.

the FTIR results of the GNPs and *A. muricata* extract. A broad and strong band observed at 3421 cm^{-1} and 3197 cm^{-1} in the *A. muricata* extract is attributed to the $N-H$ stretching of amid A and $O-H$ groups of phenols compounds, respectively. The strong peaks at 2925 cm^{-1} indicate $C-H$ stretching vibrations of alkanes and secondary amines of compounds. The peak in the 2370 cm^{-1} and 2120 cm^{-1} may be linked to the $C=N$ stretching vibration, possibly due to the use of nitrile-containing compounds as capping or stabilizing agents. While, the sharp peaks at 1633 cm^{-1} specify the $C=O$ of carbonyl groups vibrations. The strong band at 1400 cm^{-1} correspond to the $-CH_3$ groups stretching vibrations of carbohydrates in the extract. The weak peaks at 1230 cm^{-1} indicate primary amine and tertiary Amine of proteins in the extract. The band at 1058 cm^{-1} indicate the $C-O$ in-plane bending of alcohols, alkanes, esters, carboxylic acid, and ethers. The addition of $HAuCl_4$ to the *A. muricata* extract for gold nanoparticle (GNP) synthesis resulted in spectral shifts in the Fourier-transform infrared (FTIR) spectra. The FTIR spectrum of the synthesized GNPs exhibited broad peaks at 3355 cm^{-1} , and weaker peaks at 2921 , 2050 , 1623 , 1436 , 1240 , and 1058 cm^{-1} . The

presence of an Au-O band, indicative of biosynthesized GNPs, was confirmed by a peak at 666 cm^{-1} . Furthermore, the synthesis of GNPs was revealed by shifts in the multiple bands observed in the FTIR spectra of the biosynthesized GNPs. The hydroxyl groups of amines, phenolic compounds, and polyphenolic functional groups have been associated to changes in the band positions. However, the biomolecules identified in *A. muricata* extract are crucial to the stabilization and reduction of Au (III) ions to Au0 during the biosynthesis of GNPs using plant extracts (Patra and Baek 2015, Celentano et al., 2018).

3.6. X-ray Photon Spectroscopy (XPS) analysis

An XPS analysis was used to further confirm that polyphenol was present on the surface of NPs (Fig. 13). The center degrees of $Au4f_{5/2}$ and $Au4f_{7/2}$ at 88 eV and 84 eV , respectively, formed the spectra that appear in (Fig. 13A) that correspond closely to the previous reports of metallic Au^0 . However, the obtained spectra for each of the C1, N1, and O1s are analyzed in (Fig. 13B-D). The *A. muricata* extract may be the

Table 2Toxicity of *A. muricata* leaves Extract at 1st, 3rd, 5th, and 7th days.

Gross Activity	1	3	5	7
Paw licking	-	+	+	+
Salivation	-	+	+	+
Weakness	-	+	+	+
Sleep	-	+	+	+
Respiratory distress	-	-	+	+
Coma	-	-	-	+
Convulsion	-	+	+	+
Diarrhea	-	+	+	+
CNS Depression	-	-	+	+
Mortality	-	-	-	-

cause of the O1s peak at 532.3 eV, N1s peak at 399.5 eV, and C1s peak at 284.5 eV. The presence of Au with oxygen and carbon is visible in the XPS scan which provides strong evidence against biomolecules that are coated around the surface of GNPs synthesized by *A. muricata* (Rodrigues et al., 2019, Stevie and Donley 2020).

3.7. Antimicrobial study

3.7.1. Antibacterial activity

The standard nutrient agar process was used to analyze the antibacterial activity of *A. muricata* extract and *A. muricata*-GNPs under different concentrations including 15, 25, 50, and 100 $\mu\text{g}/\text{mL}$. The study

examined the antibacterial activity towards the following Gram-positive and Gram-negative bacterial strains *Bacillus subtilize* (ATCC 6633), *Streptococcus aureus* (ATCC 29213), *Staphylococcus mutants* (ATCC 25175), *Escherichia coli* (ATCC 25922), *Klebsiella pneumonia* (ATCC 13884), and *Pseudomonas aeruginosa* (ATCC 27853), respectively. Ciprofloxacin (CIP) was used as a standard antibiotic and served as both a positive and negative control. (Fig. 14). The highest level of inhibition was observed in Gram-positive bacteria *Pseudomonas aeruginosa* (ATCC 27853), exceeding the standard, while the lowest level of inhibition was observed in Gram-negative bacteria *Escherichia coli* (ATCC 25922). These significant differences in the antibacterial activity could be attributed to the Gram-negative bacterial outer membrane, which usually acts as a natural protective barrier preventing the passage of GNPs. Whereas, the out layer of Gram-positive bacterial act as good carrier for GNPs which could easily passes through outer membrane. Since green-synthesized GNPs often have higher surface area-to-volume ratios and smaller sizes which can interact with bacterial cells more effectively and intensifying their antibacterial effects. Similarly, the recent studies have demonstrated that GNPs, with their easy and affordable synthesis showed remarkable bactericidal efficiency at nanogram doses, and low toxicity that have great potential for use as antimicrobial coatings for medical fields (Al-Radadi 2023, Pikel et al., 2021).

3.7.2. Antifungal activity

The extract obtained from *A. muricata* was most lethal (17.8 ± 0.6) to *Candida albicans* and least lethal to *Aspergillus nigra* (12.8 ± 0.7). while the *A. muricata*-GNPs demonstrated the minimum activity (19.8 ± 0.5) against *Aspergillus flavus* (ATCC 16620) and the maximum activity (25 ± 0.5) against *Candida albicans* (ATCC 10231). The *A. muricata* extract and *A. muricata*-GNPs displayed extreme activity against the standard compounds and were as sensitive to the investigated fungal strains as the CIP standard antibiotics (Fig. 15). Thus, crystalline nature of GNPs exhibits significant antifungal activity by accomplished the electrostatic interactions with the pathogen cells as opposed to growth inhibition and

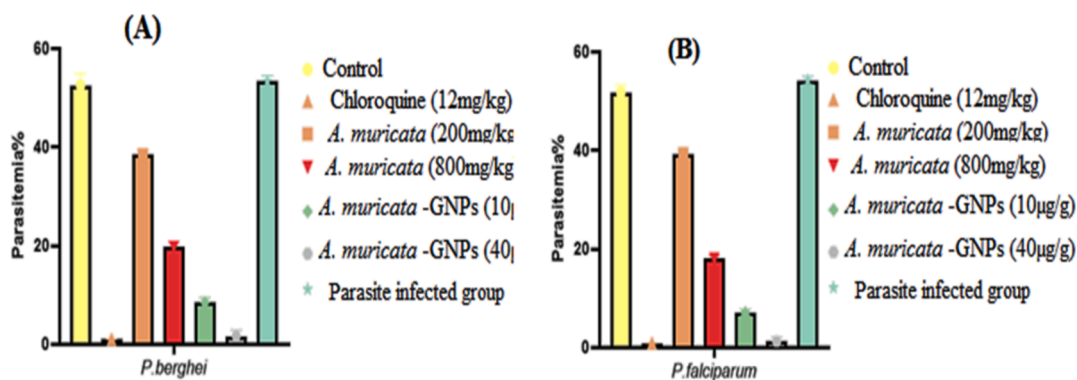


Fig. 16. Impact of *A. muricata* extract, *A. muricata*-GNPs and chloroquine on parasitemia in different experimental infected mice groups. (A) *P. berghei* infected groups. (B) *P. falciparum* infected groups.

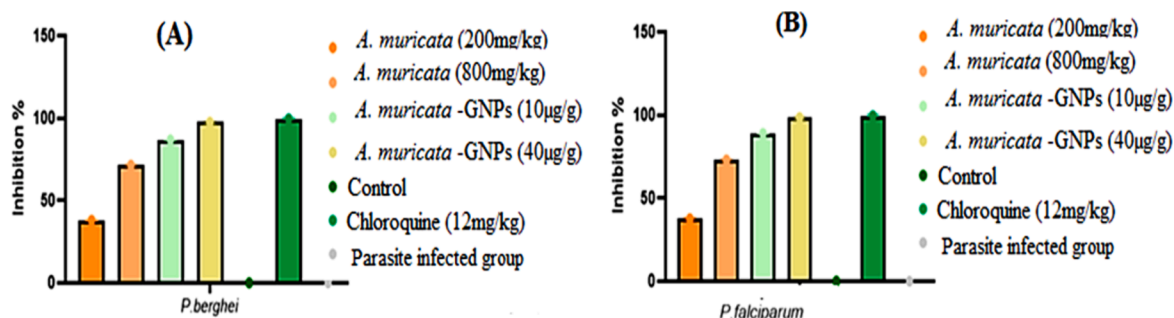


Fig. 17. The percentage of parasitic inhibition in different experimental treatment groups. (A) *P. berghei* infected groups. (B) *P. falciparum* infected groups.

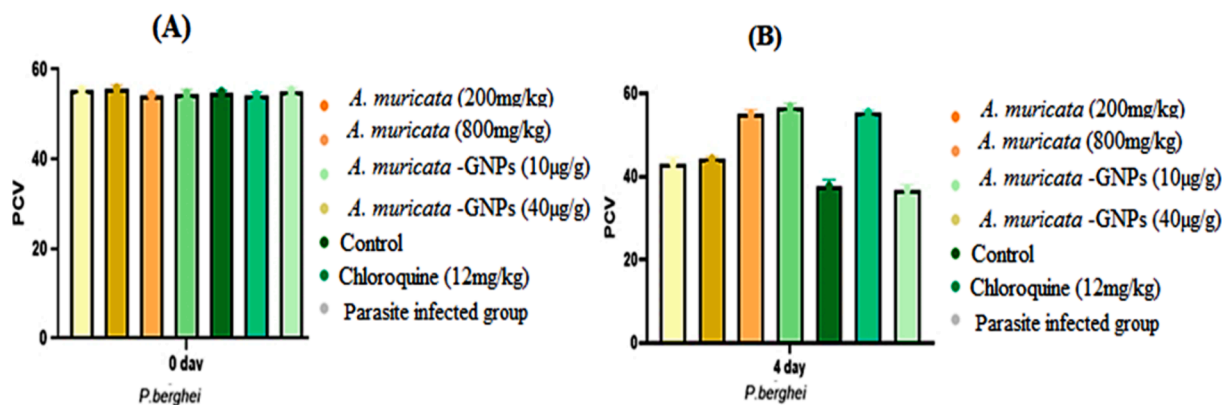


Fig. 18. Impact of time exposure on PCV in different *P. berghei* experimental infected mice groups (*A. muricata* extract, *A. muricata*-GNPs and chloroquine groups). (A) Zero day. (B) 4 days.

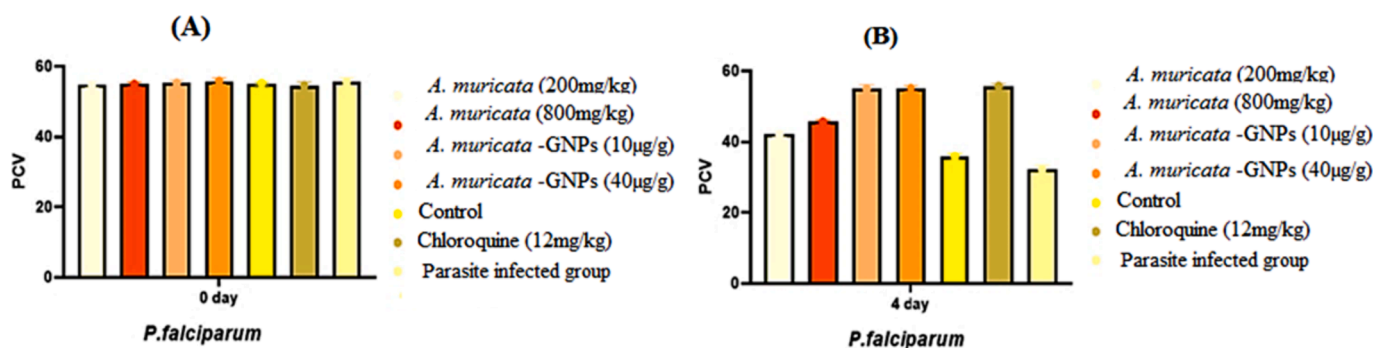


Fig. 19. Impact of time exposure on PCV in different *P. falciparum* experimental infected mice groups (*A. muricata* extract, *A. muricata*-GNPs and chloroquine groups). (A) Zero day (B) 4 days.

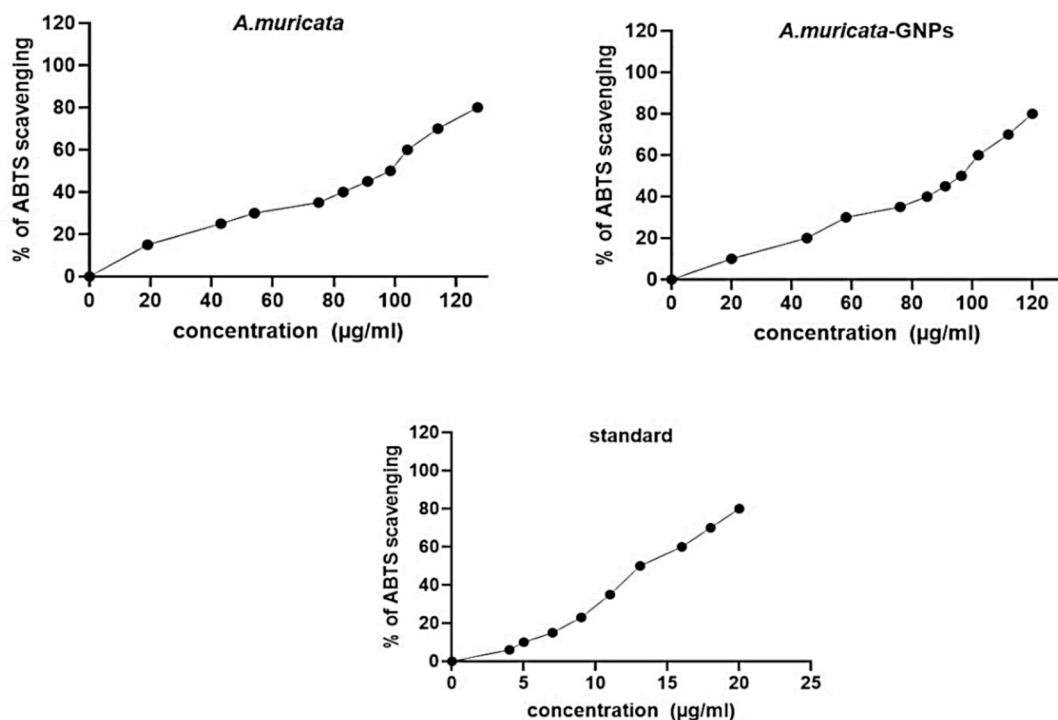


Fig. 20. Antioxidant activity of ABTS, *A. muricata* extract, *A. muricata*-GNPs, Standard.

improve the therapeutic efficiency. Therefore, GNPs were a viable option for the purpose of synthesizing an antimicrobial coating for medical application. According to the findings, gold nanoparticles have strong antifungal activity, which is consistent with earlier findings in the literature where the biogenic GNPs effectively inhibited drug-resistant fungal strains, including *Aspergillus* species, indicating their potential as a promising alternative to traditional antifungal agents (Almansob et al., 2022).

3.8. Antimalarial study

3.8.1. Acute toxicity

The administration of leaf extract of *A. muricata* into mice did not reveal any significant behavioral changes against the acute toxicity evaluation. The period of 7 days of observation showed non-mortality examination. Nevertheless, mice administered 4000 mg/kg dose showed behavioral indicators for toxicity, including paw licking, weakness, salivation, and sleep (Table 2). However, no mortality occurred at any of the prescribed doses. It appears safe because the *A. muricata* extract, up to a dose of 4000 mg/kg, did not lead to an increase in mortality within 7 days. An estimate of ≥ 2500 mg/kg was determined for the oral median LD₅₀. Thus, the obtained results showed that smaller size GNPs have a greater ability to penetrate biological barriers, and cause mitochondrial damage and oxidative stress, which ultimately results in cell necrosis. The findings suggest that the acute toxicity of GNPs can be influenced by their size and surface coating. Similarly, a prior study found that larger-size GNPs (60 nm) indicate less toxic effect, while smaller-size GNPs (13 nm) exhibit the highest toxicity by impairing mitochondrial function and inducing programmed cell death (Nižnik et al., 2024).

3.8.2. Effect of parasitemia

The common 4-day suppressive examination results for parasitemia in infected mice with *P. berghei* and *P. falciparum* were obtained in (Fig. 16). When compared to the standard group, the dose-dependent antimalarial activity was demonstrated against *P. berghei* and *P. falciparum* infection in mice that showed significant inhibition in *A. muricata*-GNPs at maximum concentrations (Fig. 17). However, the *A. muricata*-GNPs dose may have inhibited *P. falciparum* and *P. berghei* because it increased the mean survival time (MST) of the infected mice. These parasites reduced the overall pathologic effect on the mice. Whereas, *A. muricata* extracts may not possess the same level of targeting and bioavailability for the malaria parasite. This is due to the intrinsic antimalarial activity of GNPs that potentially disrupting parasite membranes or metabolic processes and enhanced overall antimalarial activity. Recent study show gold nanoparticles derived from natural plant extracts, such as marine actinobacteria, have antimalarial properties against *Plasmodium berghei* infection in mice, enhancing their survivability of infected mice compared to the control group (Karthik et al., 2013). Hence, the study found that gold nanoparticles effectively killed malaria parasites, indicating their potential as a potent antimalarial agent.

3.8.3. Effect of packed cell volume

The concentrations of *A. muricata*-GNPs revealed the highest protective effect on PCV reduction. The effect of packed cell volume on a comparison of 0–4 days was displayed in (Fig. 18) and (Fig. 19). As a result of malarial multiplication, the erythrocytes were destroyed and the infected mice developed into anemia. The extract and GNPs displayed protection towards the reduction in PCV in comparison to day 0. The results suggest that the antimalarial and antioxidant properties of the extract might be crucial.

3.9. Antioxidant activity

The ABTS assay was used to assess the antioxidant activity of an

aqueous *A. muricata* extract and *A. muricata*-GNPs. The outcomes of the ABTS radical scavenging activity are shown in (Fig. 20). The 50 % scavenging free radical activity for ABTS was demonstrated by the *A. muricata* extract at IC₅₀ (98.5 µg/mL). Whereas, the synthesized *A. muricata*-GNPs showed enhanced antioxidant activity at IC₅₀ (96.4 µg/mL) in contrast to standard that revealed IC₅₀ (13.1 µg/mL). Following a 45-minute dark incubation period at 30 °C of temperature determined the antioxidant activity of the resulting solution by using the data from earlier studies (Gavamukulya et al., 2014, Jo et al., 2017). Thus, the spherical and small size nanoparticles increase the surface area to volume ratio of GNPs demonstrated significant antioxidant activity that causes concentration-dependent reactive oxygen species production and suggesting a potential role in modulating cellular antioxidant defenses. The study found that smaller size GNPs showed higher antioxidant activity due to their increased surface area and reactivity compared to larger GNPs (Fayazbakhsh et al., 2023). Thus, the synthesized GNPs exhibit notable antioxidant activity and can be used for the treatment of oxidative stress-related disorder.

4. Conclusion

The significant novelty of this research work is to fabricate GNPs from *A. muricata* leaves extract offers a significant contribution to green synthesis and nanotechnology which are not reported in the literature. It is a simple process to perform, yields a substantial quantity of GNPs without releasing any toxic reagents into the environment, and is quick, economical can be reproducible. The synthesized GNPs were characterized using different analytical techniques, including UV-vis, FT-IR, TEM, XRD, EDX, and XPS, to identify biomolecules, morphology, crystalline nature, elemental and chemical components found in *A. muricata*-GNPs. The size and shape of GNPs fluctuate with temperature and pH, but the optimum synthesis was achieved at temperatures (25 °C) and acidic pH levels (pH 4). Furthermore, the synthesized gold nanoparticles derived from *A. muricata* leaves exhibit significant inhibition zone that was 25 ± 0.5 % against *Candida albicans* (ATCC 10231). are considered to be an effective antimicrobial agents. The study demonstrated dose-dependent antimalarial activity against *P. berghei* and *P. falciparum* infection that showed significant inhibition at maximum concentrations. Moreover, the synthesized GNPs have significant antioxidant activity which may be used as significant agent for the oxidative stress related disorders.

5. Future perspective

The effects of nanoparticles on medicine are primarily beneficial. GNP-based nanotechnology can be more successfully used to develop a stable and strong binding affinity with different kinds of targeted drugs for microbial, viral, malaria, and other disorders due to its significant therapeutic properties (Al-Radadi 2024b). Different drug companies can use the data from this study to develop antimicrobial and antimalarial medications that will aid in treating diseases for which there is no longer any effective treatment. The main limitation of *A. muricata*-GNP synthesis is currently restricted to laboratory-scale experiments, and it is challenging to apply these discoveries to large-scale manufacturing procedures. This is one of the significant issues that has to be resolved is scaling up the production of *A. muricata*-GNPs.

CRedit authorship contribution statement

Najlaa S. Al-Radadi: Writing – review & editing, Writing – original draft, Visualization, Validation, Supervision, Software, Resources, Project administration, Methodology, Investigation, Funding acquisition, Formal analysis, Data curation, Conceptualization.

References

- Abdul Wahab, S. M., I. Jantan, M. A. Haque, et al., 2018. Exploring the leaves of *Annona muricata* L. as a source of potential anti-inflammatory and anticancer agents. 9, 661.
- Abdullah, Al-Radadi, N. S., T. Hussain, S. Faisal, et al., 2022. Novel biosynthesis, characterization and bio-catalytic potential of green algae (*Spirogyra hyalina*) mediated silver nanomaterials. Saudi J. Biol. Sci. 29 (1) 411-419.
- Abdulsalami, M., V. Aina, M. Ibrahim, et al., 2016. Comparative antibacterial study of aqueous and ethanolic leaf extracts of *Annona Muricata*. 6, 141-146.
- Abid, N., Khan, A.M., Shujait, S., et al., 2022. Synthesis of nanomaterials using various top-down and bottom-up approaches, influencing factors, advantages, and disadvantages. A Review. 300, 102597.
- Ahmed, I.A., Al-Radadi, N.S., 2020. Estimating the Impact of Nanophases on the Production of Green Cement with High Performance Properties. Materials 13, 4197, doi:10.3390/ma13184197.
- Ahmed, I.A., Hussein, H.S., Ragab, A.H., Al-Radadi, N.S., 2020. Synthesis and Characterization of Silica-Coated Oxhydroxide Aluminum/Doped Polymer Nanocomposites: A Comparative Study and Its Application as a Sorbent. Molecules 25, 1520. <https://doi.org/10.3390/molecules25071520>.
- Al Jahdaly, B.A., Al-Radadi, N.S., Eldin, G.M., et al., 2021. Selenium Nanoparticles Synthesized Using an Eco-Friendly Method: Dye Decolorization from Aqueous Solutions, Cell Viability, Antioxidant, and Antibacterial Effectiveness. 11, 85–97.
- Al, O., Usman, S., Aina, O., et al., 2022. Evaluation of the Antimalarial Effects of the Leaf Extract and Fruit Juice of *Annona Muricata* against *Plasmodium Berghei* Infection in Mice. 1.
- Al-Ahmed, Z.A., Al-Radadi, N.S., Ahmed, M.K., Shouei, K., El-Kemary, M., 2020. Dye removal, antibacterial properties, and morphological behavior of hydroxyapatite doped with Pd ions. Arab. J. Chem. 13 (12), 8626–8637.
- Almansob, A., Bahkali, A.H., Ameen, F., 2022. Efficacy of gold nanoparticles against drug-resistant nosocomial fungal pathogens and their extracellular enzymes: resistance profiling towards established antifungal agents. Nanomater. 12, 814.
- Al-Radadi, N.S., 2019. Green synthesis of platinum nanoparticles using Saudi's Dates extract and their usage on the cancer cell treatment. Arab. J. Chem. 12 (3), 330–349.
- Al-Radadi, N.S., 2021a. Facile one-step green synthesis of gold nanoparticles (AuNP) using licorice root extract: Antimicrobial and anticancer study against HepG2 cell line. Arab. J. Chem. 14 (2), 102956.
- Al-Radadi, N.S., 2021b. Green biosynthesis of flaxseed gold nanoparticles (Au-NPs) as potent anti-cancer agent against breast cancer cells. J. Saud. Chem. Soci. 25 (6), 101243.
- Al-Radadi, N.S., 2022a. *Saussurea costus* for sustainable and eco-friendly synthesis of palladium nanoparticles and their biological activities. Arab. J. Chem. 15 (11), 104294.
- Al-Radadi, N.S., 2022b. Biogenic proficient synthesis of (Au-NPs) via aqueous extract of Red Dragon Pulp and seed oil: Characterization, antioxidant, cytotoxic properties, anti-diabetic anti-inflammatory, anti-Alzheimer and their anti-proliferative potential against cancer cell lines. Saudi J. Biol. Sci. 29 (4), 2836–2855.
- Al-Radadi, N.S., 2022c. Laboratory scale medicinal plants mediated green synthesis of biocompatible nanomaterials and their versatile biomedical applications. Saudi J. Biol. Sci. 29 (5), 3848–3870.
- Al-Radadi, N.S., 2022d. Microwave assisted green synthesis of Fe@ Au core-shell NPs magnetic to enhance olive oil efficiency on eradication of *helicobacter pylori* (life preserver). Arab. J. Chem. 15 (5), 103685.
- Al-Radadi, N.S., 2022e. Single-step green synthesis of gold conjugated polyphenol nanoparticle using extracts of Saudi's myrrh: Their characterization, molecular docking and essential biological applications. Saudi Pharm. J. 30 (9), 1215–1242.
- Al-Radadi, N.S., 2023. Ephedra mediated green synthesis of gold nanoparticles (AuNPs) and evaluation of its antioxidant, antipyretic, anti-asthmatic, and antimicrobial properties. Arab. J. Chem. 16 (1), 104353.
- Al-Radadi, N. S., 2018. Artichoke (*Cynara scolymus* L.) mediated rapid analysis of silver nanoparticles and their utilisation on the cancer cell treatments. J. Comput. Theor. Nanosci. 15 (6-7), 1818-1829.
- Al-Radadi, N.S., 2024a. Physicochemical characterization of *Glycyrrhiza* mediated bioengineered palladium nanoparticles (PdNPs), their anti-proliferative and other biomedical applications. Journal of King Saud University - Science 36 (7), 103256.
- Al-Radadi, N.S., 2024b. Therapeutic Evaluation of Nano-Formulated Extract against the Interplay between Inflammation and Oxidative Stress in Experimental Models of Type 2 Diabetes. Journal of King Saud University - Science 37.
- Al-Radadi, N.S., Abu-Dief, A.M., 2022. Silver nanoparticles (AgNPs) as a metal nanotherapy: possible mechanisms of antiviral action against COVID-19. Inorg. Nano-Met. 1–19.
- Al-Radadi, N.S., Adam, S.I., 2020. Green biosynthesis of Pt-nanoparticles from Anbara fruits: toxic and protective effects on CCl4 induced hepatotoxicity in Wistar rats. Arab. J. Chem. 13 (2), 4386–4403.
- Al-Radadi, N. S. and A. N. Al-Youbi, 2018a. One-step synthesis of au nano-assemblies and study of their anticancer activities. J. Comput. Theor. Nanosci. 15 (6-7), 1861-1870.
- Al-Radadi, N.S., Faisal, S., Alotaibi, A., et al., 2022. Zingiber officinale driven bioproduction of ZnO nanoparticles and their anti-inflammatory, anti-diabetic, anti-Alzheimer, anti-oxidant, and anti-microbial applications. Inorg. Chem. Commun. 140, 109274.
- Al-Radadi, N.S., AlBishri, Widad, M., ElShebiny, Shaimaa A., Salem, Neveen A., 2024. Plant-Mediated Green Synthesis of Gold Nanoparticles Using an Aqueous Extract of *Passiflora ligularis*, Optimization, Characterizations, and their Neuroprotective Effect on Propionic Acid-Induced Autism in Wistar Rats. Saudi Pharm. J. 32 (2) 101921.
- Amani, A.M., Danaie, P., Vaez, A., et al., 2022. Rutin precursor for the synthesis of superparamagnetic ZnFe₂O₄ nanoparticles: Experimental and density functional theory. Appl. Phys. a. 128, 696.
- Anderson, S.D., Gwenin, V.V., Gwenin, C.D., 2019. Magnetic functionalized nanoparticles for biomedical, drug delivery and imaging applications. Nanoscale Res. Lett. 14 (1–16).
- Asase, A., Hesse, D.N., Simmonds, M.S., 2012. Uses of multiple plants prescriptions for treatment of malaria by some communities in southern Ghana. J. Ethnopharmacol. 144 (2), 448–452.
- Attarilar, S., Yang, J., Ebrahimi, M., et al., 2020. The toxicity phenomenon and the related occurrence in metal and metal oxide nanoparticles: a brief review from the biomedical perspective. Front. Bioeng. Biotechnol. 8, 822.
- Badeggi, U.M., Ismail, E., Adeloye, A.O., et al., 2020. Green synthesis of gold nanoparticles capped with procyanidins from *Leucosidea sericea* as potential antidiabetic and antioxidant agents. Biomolecules. 10 (3), 452.
- Balasubramanian, S.K., Yang, L., Yung, L.-Y.-L., et al., 2010. Characterization, purification, and stability of gold nanoparticles. Biomaterial. 31 (34), 9023–9030.
- Balderrama-Carmona, A.P., Silva-Beltrán, N.P., Gálvez-Ruiz, J.-C., et al., 2020. Antiviral, antioxidant, and antihemolytic effect of *Annona muricata* L. leaves extracts. Plants. 9 (12), 1650.
- Balfourier, A., Kolosnjaj-Tabi, J., Luciani, N., et al., 2020. Gold-based therapy: From past to present. PNAS. 117 (37), 22639–22648.
- Basavegowda, N., Baek, K.-H., 2021. Multimetallic nanoparticles as alternative antimicrobial agents: challenges and perspectives. Int J Nanomedicine. 26 (4), 912.
- Bharadwaj, K.K., Rabha, B., Pati, S., et al., 2021. Green synthesis of gold nanoparticles using plant extracts as beneficial prospect for cancer theranostics. Molecules. 26 (21), 6389.
- Boroumand Moghaddam, A., Namvar, F., Moniri, M., et al., 2015. Nanoparticles biosynthesized by fungi and yeast: a review of their preparation, properties, and medical applications. Molecules. 20 (9), 16540–16565.
- Celentano, M., Jakhmola, A., Profeta, M., et al., 2018. Diffusion limited green synthesis of ultra-small gold nanoparticles at room temperature. Colloids Surf. a: Physicochem. Eng. 558, 548–557.
- Chan, W.-J.-J., McLachlan, A.J., Hanrahan, J.R., et al., 2020. The safety and tolerability of *Annona muricata* leaf extract: a systematic review. J. Pharm. Pharmacol. 72 (1), 1–16.
- Cho, K., Wang, X., Nie, S., et al., 2008. Therapeutic nanoparticles for drug delivery in cancer. Clin. Cancer Res. 14 (5), 1310–1316.
- Choi, J.-H., Ohk, S.-H., 2017. Evaluations on Antioxidant Effect of Water Extract from *Graviola* Leaves. J. Korean Acad. Nurs. 18 (6), 129–135.
- Chowdhury, S.S., Tareq, A.M., Tareq, S.M., et al., 2021. Screening of antidiabetic and antioxidant potential along with phytochemicals of *Annona* genus: A review. Future J. Pharm. Sci. 7, 1–10.
- Coria-Téllez, A.V., Montalvo-González, E., Yahia, E.M., et al., 2018. *Annona muricata*: A comprehensive review on its traditional medicinal uses, phytochemicals, pharmacological activities, mechanisms of action and toxicity. Arab. J. Chem. 11 (5), 662–691.
- Costa, E. V., M. L. B. Pinheiro, J. R. d. A. Silva, et al., 2009. Antimicrobial and antileishmanial activity of essential oil from the leaves of *Annona foetida* (Annonaceae). Quim. Nova. 32, 78-81.
- Desai, N., Momin, M., Khan, T., et al., 2021. Metallic nanoparticles as drug delivery system for the treatment of cancer. Expert Opin. Drug Deliv. 18 (9), 1261–1290.
- Dong, J., Carpinone, P.L., Pyrgiotakis, G., et al., 2020. Synthesis of precision gold nanoparticles using Turkevich method. KONA Powder Part. J. 37, 224–232.
- Donga, S., Bhadu, G.R., Chanda, S., 2020. Antimicrobial, antioxidant and anticancer activities of gold nanoparticles green synthesized using *Mangifera indica* seed aqueous extract. Artif. Cells Nanomed. Biotechnol. 48 (1), 1315–1325.
- Dung, N.T., Linh, N.T., Chi, D.L., et al., 2021. Optical properties and stability of small hollow gold nanoparticles. RSC Adv. 11 (22), 13458–13465.
- Elahi, N., Kamali, M., Baghersad, M.H., 2018. Recent biomedical applications of gold nanoparticles: A review. Talanta. 184, 537–556.
- Faisal, S., Al-Radadi, N. S., T. Hussain, Abdullah, et al., 2021. Curcuma longa Mediated Synthesis of Copper Oxide, Nickel Oxide and Cu-Ni Bimetallic Hybrid Nanoparticles: Characterization and Evaluation for Antimicrobial, Anti-Parasitic and Cytotoxic Potentials. Coatings 2021, 11, 849.
- Fayazbakhsh, F., Hataminia, F., Eslam, H.M., et al., 2023. Evaluating the antioxidant potential of resveratrol-gold nanoparticles in preventing oxidative stress in endothelium on a chip. Sci. Rep. 13, 21344.
- Folorunso, A., Akintelu, S., Oyebamiji, A.K., et al., 2019. Biosynthesis, characterization and antimicrobial activity of gold nanoparticles from leaf extracts of *Annona muricata*. J. Nanostructure Chem. 9, 111–117.
- Gajalakshmi, S., Vijayalakshmi, S., Devi, R.V., 2012. Phytochemical and pharmacological properties of *Annona muricata*: a review. Int. J. Pharm. Sci. 4 (2), 3–6.
- García Durán, A., M. T. Gutiérrez Vázquez, F. J. Rodríguez Mejías, et al., 2021. An Overview of the Chemical Characteristics, Bioactivity and Achievements Regarding the Therapeutic Usage of Acetogenins from *Annona cherimola* Mill.
- Gavamukulya, Y., Abou-Ellella, F., Wamunyokoli, F., et al., 2014. Phytochemical screening, anti-oxidant activity and in vitro anticancer potential of ethanolic and water leaves extracts of *Annona muricata* (*Graviola*). Asian Pac. J. Trop. Med. 7, S355–S363.
- Gavamukulya, Y., Wamunyokoli, F., El-Shemy, H.A., 2017. *Annona muricata*: Is the natural therapy to most disease conditions including cancer growing in our backyard? A systematic review of its research history and future prospects. Asian Pac. J. Trop. Med. 10 (9), 835–848.
- Haldar, K., Mohandas, N., 2009. Malaria, erythrocytic infection, and anemia. ASH Education Program Book. 1, 87–93.

- Hlavkova, D., Caloudova, H., Palikova, P., Kopel, P., Plhalova, L., Beklova, M., Havelkova, B., 2020. Effect of gold nanoparticles and ions exposure on the aquatic organisms. *Bulletin of Environmental Contamination and Toxicology* 105, 530–537.
- Iyanda-Joel, W. O., E. A. Omonigbehin, E. E. Iweala, et al., 2019. Antibacterial studies on fruit-skin and leaf extracts of *Annona muricata* in Ota, Nigeria. IOP Conference Series: Earth and Environmental Science, IOP Publishing.
- Janse, C.J., Ramesar, J., Waters, A.P., 2006. High-efficiency transfection and drug selection of genetically transformed blood stages of the rodent malaria parasite *Plasmodium berghei*. *Nat. Protoc.* 1 (1), 346–356.
- Javed, R., Zia, M., Naz, S., et al., 2020. Role of capping agents in the application of nanoparticles in biomedicine and environmental remediation: recent trends and future prospects. *J. Nanobiotechnology*. 18, 1–15.
- Jo, E.H., Kim, I.H., Lee, J.H., 2017. Antioxidant and skin whitening effect of graviola (*Annona muricata*) leaf extracts. *Appl. Chem. Eng.* 28 (2), 198–205.
- Kajani, A.A., Bordbar, A.-K., Esfahani, S.H.Z., et al., 2016. Gold nanoparticles as potent anticancer agent: green synthesis, characterization, and in vitro study. *RSC Adv.* 6 (68), 63973–63983.
- Karthik, L., Kumar, G., Keswani, T., et al., 2013. Marine actinobacterial mediated gold nanoparticles synthesis and their antimalarial activity. *Nanomedicine: Nanotechnology, Biology and Medicine (NBM)*. 9, 951–960.
- Khan, M.A.R., Al Mamun, M.S., Habib, M.A., et al., 2022. A review on gold nanoparticles: biological synthesis, characterizations, and analytical applications. *Results Chem.* 100478.
- Lachowicz, J.I., Lecca, L.I., Meloni, F., et al., 2021. Metals and metal-nanoparticles in human pathologies: from exposure to therapy. *Molecules*. 26 (21), 6639.
- Lorke, D. J. A. o. t., 1983. A new approach to practical acute toxicity testing. *54*, 275–287.
- Luo, J., Zhang, Y., Zhu, S., et al., 2021. The application prospect of metal/metal oxide nanoparticles in the treatment of osteoarthritis. *Naunyn-Schmiedeberg's Arch. Pharmacol.* 394 (10), 1991–2002.
- Makeri, H., Maikai, V., Muhammad, A., 2015. Evaluation of antibacterial activities of Graviola (*Annona muricata*) leave and stem bark extracts against clinical isolates of *Salmonella* spp and *Escherichia coli*. *BAJOPAS*. 8 (1), 143–148.
- Maraming, P., Daduang, J., Kah, J.C.Y., 2022. Conjugation with gold nanoparticles improves the stability of the KT2 peptide and maintains its anticancer properties. *RSC Adv.* 12 (1), 319–325.
- Martínez, J., Chequer, N., González, J., et al., 2012. Alternative methodology for gold nanoparticles diameter characterization using PCA technique and UV-VIS spectrophotometry. *Nanosci. Nanotechnol.* 2 (6), 184–189.
- Mishra, A.P., Nigam, M., Namboozee, J., et al., 2023. GC-MS Analysis, Antioxidant, and Antidiabetic Properties of Methanol Extract of *Annona muricata* L. Leaves-An In vitro and In silico Study. *Curr. Org. Chem.* 27, 1531–1541.
- Mitchell, M.J., Billingsley, M.M., Haley, R.M., et al., 2021. Engineering precision nanoparticles for drug delivery. *Nat. Rev. Drug Discov.* 20 (2), 101–124.
- Moghadamzadeh, S.Z., Fadaeinasab, M., Nikzad, S., et al., 2015. *Annona muricata* (Annonaceae): a review of its traditional uses, isolated acetogenins and biological activities. *Int. J. Mol. Sci.* 16 (7), 15625–15658.
- Mohammed, A., Ndaro, A., Kalinga, A., et al., 2013. Trends in chloroquine resistance marker, Pfcrt-K76T mutation ten years after chloroquine withdrawal in Tanzania. *Malar. J.* 12 (1), 1–7.
- Mughal, B., Zaidi, S.Z.J., Zhang, X., et al., 2021. Biogenic nanoparticles: Synthesis, characterisation and applications. *Appl. Sci.* 11 (6), 2598.
- Mutakin, M., Fauziati, R., Fadhilah, F.N., et al., 2022. Pharmacological activities of soursop (*Annona muricata* Linn.). *Molecules*. 27 (4), 1201.
- Nguyen, M., Nguyen, V., Minh, L., et al., 2020. Determination of the Phytochemical Screening, Total Polyphenols, Flavonoids Content, and Antioxidant Activity of Soursop Leaves (*Annona muricata* Linn.). IOP Publishing.
- Niznik, L., Noga, M., Kobylarz, D., et al., 2024. Gold Nanoparticles (AuNPs)—Toxicity, Safety and Green Synthesis: A Critical Review. *Int. J. Mol. Sci.* 25, 4057.
- Nuwaha, F., 2001. The challenge of chloroquine-resistant malaria in sub-Saharan Africa. *Health policy*.
- Paarakh, P.M., Chansouria, J., Khosa, R., 2009. Wound healing activity of *Annona muricata* extract. *J. Pharm. Res.* 2 (3), 404–406.
- Parija, S., Praharaj, I., 2011. Drug resistance in malaria. *Indian J. Med. Microbiol.* 29 (3), 243–248.
- Patra, J.K., Baek, K.-H., 2015. Novel green synthesis of gold nanoparticles using *Citrullus lanatus* rind and investigation of proteasome inhibitory activity, antibacterial, and antioxidant potential. *Int J Nanomedicine*. 7253–7264.
- Paul, K., Bag, B.G., Samanta, K., 2014. Green coconut (*Cocos nucifera* Linn) shell extract mediated size controlled green synthesis of polyshaped gold nanoparticles and its application in catalysis. *Appl. Nanosci.* 4, 769–775.
- Peters, W., Portus, J., Robinson, B., 1975. The chemotherapy of rodent malaria, XXII: the value of drug-resistant strains of *P. berghei* in screening for blood schizontocidal activity. *Ann. Trop. Med. Parasitol.* 69 (2), 155–171.
- Pieme, C.A., Kumar, S.G., Dongmo, M.S., et al., 2014. Antiproliferative activity and induction of apoptosis by *Annona muricata* (Annonaceae) extract on human cancer cells. *BMC Complement Altern. Med.* 14 (1), 1–10.
- Piktel, E., Suprewicz, L., Depciuch, J., et al., 2021. Varied-shaped gold nanoparticles with nanogram killing efficiency as potential antimicrobial surface coatings for the medical devices. *Sci. Rep.* 11, 12546.
- Priya MR, K. and P. R. Iyer, 2020. Antiproliferative effects on tumor cells of the synthesized gold nanoparticles against Hep2 liver cancer cell line. *Egypt. Liver J.* 10, 1–12.
- Rady, I., Bloch, M.B., Chamcheu, R.-C.-N., et al., 2018. Anticancer properties of graviola (*Annona muricata*): a comprehensive mechanistic review. *Oxidative Med. Cell. Longev.* p. 2018.
- Rodrigues, T.S., da Silva, A.G., Camargo, P.H., 2019. Nanocatalysis by noble metal nanoparticles: controlled synthesis for the optimization and understanding of activities. *J. Mater. Chem.* 7 (11), 5857–5874.
- Sargazi, S., Laraib, U., Er, S., et al., 2022. Application of green gold nanoparticles in cancer therapy and diagnosis. *Nanomater.* 12 (7), 1102.
- Shabani, L., Kasaei, S.R., Chelliapan, S., et al., 2023. An investigation into green synthesis of Ru template gold nanoparticles and the in vitro photothermal effect on the MCF-7 human breast cancer cell line. *Appl. Phys. a*. 129, 564.
- Sharma, H., Kumar, K., Choudhary, C., et al., 2016. Development and characterization of metal oxide nanoparticles for the delivery of anticancer drug. *Artif. Cells Nanomed.* 44 (2), 672–679.
- Soleimani Zohr Shiri, M., W. Henderson and M. R. Mucalo, 2019. A review of the lesser-studied microemulsion-based synthesis methodologies used for preparing nanoparticle systems of the noble metals, Os, Re, Ir and Rh. *Materials*. 12 (12), 1896.
- Shmarakov, I., Mukha, I., Vityuk, N., et al., 2017. Antitumor activity of alloy and core-shell-type bimetallic AgAu nanoparticles. *Nanoscale Res. Lett.* 12, 1–10.
- Singh, P., Mijakovic, I., 2021. Advances in gold nanoparticle technology as a tool for diagnostics and treatment of cancer. *Expert Rev. Mol. Diagn.* 21 (7), 627–630.
- Somsak, V., N. Polwiang and S. Chachiyu, 2016. In vivo antimalarial activity of *Annona muricata* leaf extract in mice infected with *Plasmodium berghei*. *J. Pathog.* 2016.,
- Son, Y., Lee, H., Son, S.-Y., et al., 2021. Ameliorative effect of *Annona muricata* (Graviola) extract on hyperglycemia induced hepatic damage in Type 2 diabetic mice. *Antioxid.* 10 (10), 1546.
- Stevie, F.A., Donley, C.L., 2020. Introduction to x-ray photoelectron spectroscopy. *J. Vac. Sci. Technol.* 38 (6).
- Swain, S., Barik, S., Behera, T., et al., 2016. Green synthesis of gold nanoparticles using root and leaf extracts of *Vetiveria zizanioides* and *Cannabis sativa* and its antifungal activities. *J. Bionanosci.* 6, 205–213.
- Taib, S.H.M., Shameli, K., Nia, P.M., et al., 2019. Electrooxidation of nitrite based on green synthesis of gold nanoparticles using *Hibiscus sabdariffa* leaves. *J. Taiwan Inst. Chem.* 95, 616–626.
- Tyagi, P.K., Quispe, C., Herrera-Bravo, J., et al., 2021. Synthesis of silver and gold nanoparticles: Chemical and green synthesis method and its toxicity evaluation against pathogenic bacteria using the toxtrak test. *J. Nanomater.* 2021, 1–12.
- Vijayameena, C., Subhashini, G., Loganayagi, M., et al., 2013. Original Research Article Phytochemical screening and assessment of antibacterial activity for the bioactive compounds in *Annona muricata*. *J. Curr. Microbiol. Appl. Sci.* 2, 1–8.
- White, B., Banerjee, S., O'Brien, S., et al., 2007. Zeta-potential measurements of surfactant-wrapped individual single-walled carbon nanotubes. *J. Phys. Chem. c*. 111 (37), 13684–13690.
- Xu, J.-J., Zhang, W.-C., Guo, Y.-W., et al., 2022. Metal nanoparticles as a promising technology in targeted cancer treatment. *Drug Deliv.* 29 (1), 664–678.